

# **SELF REPORT**

*Panagiotis Theodorakis*

Attachment 3

Warsaw, 22 March 2021

## Table of Contents

<b>1. Name and surname</b> .....	<b>3</b>
<b>2. Education and degrees</b> .....	<b>3</b>
<b>3. Information on employment</b> .....	<b>3</b>
<b>4. Bibliometric summary of scientific publications</b> .....	<b>3</b>
<b>5. Scientific achievement being the basis of the Habilitation thesis</b> .....	<b>4</b>
<b>5.1 Title of the scientific achievement</b> .....	<b>4</b>
<b>5.2 List of publications constituting the scientific achievement</b> .....	<b>4</b>
<b>5.3 Description of the scientific objectives and the research results presented in publications H1–H5 together with the discussion of their possible applications</b> .....	<b>4</b>
<b>5.3.1 Superspreading (H1–H3)</b> .....	<b>5</b>
<b>5.3.2 Durotaxis (H4)</b> .....	<b>10</b>
<b>5.3.3 Surface Nanobubbles (H5)</b> .....	<b>13</b>
<b>5.3.4 Summary of the significance of publications H1–H5</b> .....	<b>15</b>
<b>5.3.5 References</b> .....	<b>16</b>
<b>6. Discussion of other scientific achievements</b> .....	<b>18</b>
<b>6.1 Description of research not contributing directly to the Habilitation thesis</b> .....	<b>18</b>
<b>6.2 Oral presentations</b> .....	<b>26</b>
<b>6.3 Principal investigator of research projects at IPPAS</b> .....	<b>28</b>
<b>6.4 Fellowships and awards</b> .....	<b>29</b>
<b>6.5 Research visits (minimum 1 month)</b> .....	<b>29</b>
<b>6.6 Visiting Researcher</b> .....	<b>29</b>
<b>7. Service to academic community</b> .....	<b>29</b>
<b>7.1 Reviewer activity</b> .....	<b>29</b>
<b>7.2 Memberships</b> .....	<b>30</b>
<b>7.3 Teaching activities</b> .....	<b>30</b>
<b>7.4 Participation in Examining Committees</b> .....	<b>30</b>
<b>7.5 Activity as an editor</b> .....	<b>30</b>
<b>7.6 Activities popularising science</b> .....	<b>30</b>

## 1. Name and surname

Panagiotis Theodorakis

## 2. Education and degrees

- **PhD** in Materials Science and Engineering  
Department of Materials Science and Engineering, University of Ioannina, **Greece** (2008)  
Dissertation title: *Monte Carlo simulation of polymer blends with variable architecture*  
Executive Supervisor: Prof. Constantinos Vlahos  
Formal Supervisor: Prof. Apostolos Avgeropoulos
- **Diploma** in Materials Science and Engineering  
Department of Materials Science and Engineering, University of Ioannina, **Greece** (2004)  
Diploma thesis title: *Study of carbon nanotubes with theoretical and computer simulation methods*  
Supervisor: Prof. Efthimios Kaxiras

## 3. Information on employment

- October 2015 – present: *Assistant Professor*, Institute of Physics of the Polish Academy of Sciences, Warsaw, **Poland**
- January 2013 – October 2015: *Research Associate*, Imperial College London, London, **United Kingdom** (with Prof. Omar Matar, Prof. Richard Craster, and Prof. Erich Müller)
- November 2010 – October 2012: *Postdoctoral Researcher*, University of Vienna and Technical University of Vienna, Vienna, **Austria** (with Prof. Christoph Dellago and Prof. Gerhard Kahl)
- March 2008 – October 2010: *Max Planck Fellow*, Max Planck Institute for Polymer Research and Johannes Gutenberg-University Mainz, Mainz, **Germany** (with Prof. Kurt Binder and Prof. Wolfgang Paul)

## 4. Bibliometric summary of scientific publications

Open Researcher and Contributor ID (ORCID): **0000-0002-0433-9461**

Bibliometric data:

- Web of Science (22 March 2021):
  - Researcher ID: **B-4019-2011**
  - Number of articles with citation data: **64**
  - Total number of citations: **789** (639 without self-citations)
  - Hirsch index: **16**
- Google Scholar (22 March 2021):
  - Total number of citations: **1039**
  - Hirsch index: **20**
  - i-10 index: **35**

## 5. Scientific achievement being the basis of the Habilitation thesis

### 5.1 Title of the scientific achievement

*Nanodroplets and Nanobubbles on Solid Substrates: Molecular Dynamics Simulation of Interfacial Phenomena.*

### 5.2 List of publications constituting the scientific achievement

**H1. P. E. Theodorakis**, E. A. Müller, R. V. Craster, O. K. Matar, “Modelling the superspreading of surfactant-laden droplets with computer simulation”, *Soft Matter* 11, 9254 (2015)

**H2. P. E. Theodorakis**, E. A. Müller, R. V. Craster, O. K. Matar, “Superspreading: Mechanisms and molecular design”, *Langmuir* 31, 2304 (2015)

**H3. P. E. Theodorakis**, E. R. Smith, E. A. Müller, “Spreading of aqueous droplets with common and superspreading surfactants. A molecular dynamics study”, *Colloids and Surfaces A: Physicochemical and Engineering Aspects* 581, 123810 (2019)

**H4. P. E. Theodorakis**, S. A. Egorov, A. Milchev, “Stiffness-guided motion of a droplet on a solid substrate”, *Journal of Chemical Physics* 146, 244705 (2017)

**H5. Z. Che, P. E. Theodorakis**, “Formation, dissolution, and properties of surface nanobubbles”, *Journal of Colloid and Interface Science* 487, 123 (2017)

### 5.3 Description of the scientific objectives and the research results presented in publications H1–H5 together with the discussion of their possible applications

Nanodroplets and nanobubbles at the interface with solid substrates can lead to impressive phenomena, which are relevant for a wide range of applications, such as coating technology, drug and herbicides delivery, enhanced oil recovery, drag reduction, catalysis and electrolysis, and transport in nanofluidic devices [1–3]. In particular, surfactant-laden aqueous droplets can unexpectedly fast and completely wet hydrophobic substrates, which is known as *superspreading* [H1–H3]. Liquid droplets can autonomously move on substrates with stiffness gradient, which is known as *durotaxis* [H4]. *Surface nanobubbles* can remain stable on solid substrates for hours or even days beyond any theoretical expectation (Rayleigh–Plesset theory) that would suggest that they should dissolve in sub-second time scales [H5]. Despite extensive research, numerous fundamental questions had remained open regarding the physical mechanisms and the different factors that dictate these interfacial phenomena. Molecular dynamics simulation is perfectly suited for addressing these issues, since it can access the molecular-scale detail required to describe these phenomena, in contrast to continuum simulation and experiment [4–7]. Here, I discuss main results, obtained by molecular dynamics simulation based on all-atom and coarse-grained models, which have advanced our understanding of these interfacial phenomena for nanodroplets and nanobubbles on solid substrates [H1–H5].

Our simulations have unravelled the superspreading mechanism of droplets laden with superspreading surfactants [H1–H3], which had remained elusive for more than six decades, despite the extensive research from experiment and continuum simulation [8,9]. Moreover, we have identified key properties for surfactants that can lead to superspreading behaviour and clarified the role of these properties in the superspreading process. This can result in the informed design of surfactants for tailor-made applications that require efficient spreading, such as coating and herbicides technology [1].

By using molecular dynamics simulations of a coarse-grained model, we have also been able to elucidate the microscopic mechanisms of the durotaxis motion of liquid droplets on solid substrates with stiffness gradient, in this way suggesting designs for the droplets and the substrate that enable the optimisation of this process, such as the choice of the stiffness gradient and the substrate wettability, as well as the size and the viscosity of the droplets [H4]. This work bears the potential of impacting a range of applications that require the control of droplet motion, such as

microfluidic devices and microreactors [10]. Interestingly, this has broader implications for understanding the durotaxis motion in other systems, such as the motion of living cells on tissues [11].

Finally, we have used molecular dynamics simulations of all-atom force-fields to investigate the formation, dissolution, and various properties of surface nanobubbles on solid substrates [H5]. In particular, the molecular-level simulations have been able to resolve the formation and dissolution mechanisms of surface nanobubbles and identify the role of different parameters in their stability. Moreover, we have been able to measure key properties of surface nanobubbles, such as the density and the surface tension of their gas phase, which pose significant challenges for experiment [R1]. In this way, our study has been able to provide fundamental knowledge of the behaviour of surface nanobubbles, which is relevant for applications, such as flotation, nanocomposite foams, plasmonics, boiling heat transfer devices, nanoporous films, drag reduction, *etc.* [12–19].

### 5.3.1 Superspreading (H1–H3)

Superspreading is the unexpectedly fast and complete spreading of surfactant-laden aqueous droplets on hydrophobic substrates [1,20,R2]. The surfactants that lead to this phenomenon are known as superspreaders. The most popular superspreaders are trisiloxane surfactants, which have a hydrophobic trisiloxane head and a hydrophilic alkyl ether tail (**Figure 1**) [21]. The latter hydrophilic group is also present in conventional surfactants. In addition, trisiloxane superspreading surfactants have a characteristic T-shape structure with respect to the conventional surfactants that usually have a linear molecular architecture. While in the case of conventional surfactants, the increase of the droplet radius,  $R$ , with time,  $t$ , during spreading scales as  $R \sim t^a$ , where the spreading exponent  $a \approx 0.1$  (Tanner's law), in the case of superspreaders,  $a$  can be as large as unity (**Figure 2**). Such values have been reported in both experiments [22,23] and numerical and molecular simulations [5,H2]. Other characteristics of the superspreading behaviour is the dependence of the spreading rate and the droplet contact angle on surfactant concentration. Both properties do not monotonically depend on the increase of concentration, but both initially increase with the surfactant concentration and then decrease upon further increase of the concentration [22]. Experiments have also investigated the effects of different factors that influence superspreading (*e.g.* rate of evaporation [24], humidity [25], pH [26], influence of surfactant structure and concentration [27,28], surfactant aging effects [29], behaviour of surfactant mixtures [30,31], substrate hydrophobicity [25,32], and temperature [27,38]), but the superspreading mechanism and the key design features of superspreaders had largely remained unknown.

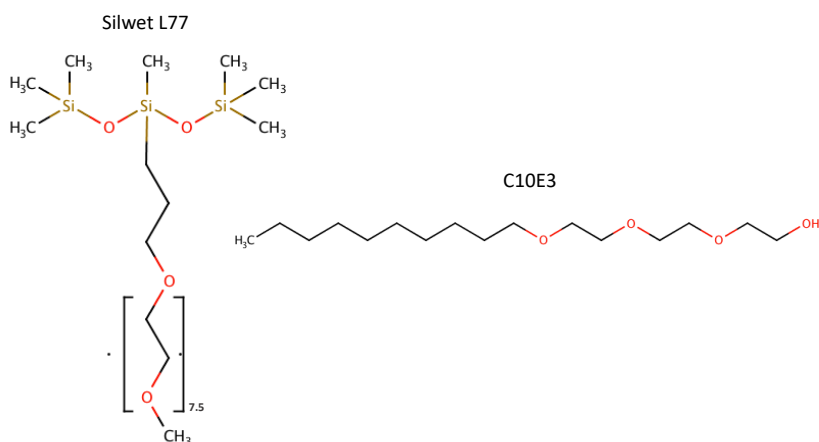


**Figure 1 Left panel:** Structure of the superspreading (T3E7.5) trisiloxane surfactant (commercial name: Silwet-L77), which has a T shape and consists of three siloxane groups (hydrophobic head) and a hydrophilic tail of 7.5 ethoxyl groups; **Right panel:** Structure of a common linear surfactant C10E3 consisting of ten alkane (hydrophobic) and three ethoxyl (hydrophilic) groups. In our studies, we have considered various surfactants, such as T shape surfactants with a smaller tail, for example, T3E3, as well as various common linear surfactants, such as C10E8, C12E5, and C12E6. Figure from Ref. H3.

In view of the large spectrum of applications of the superspreading phenomenon, we have attempted to address these issues at the molecular scale by carrying out molecular dynamics simulations based on coarse-grained models. The choice of a coarse-grained model allowed for accessing adequately large droplet sizes and time scales, which are both crucial to capture the surfactant transport processes within the droplet, which actually constitute the underlying superspreading mechanism. In contrast to continuum modelling and theory [5], molecular simulation can provide the microscopic detail of the system by tracking the position of each molecule at any time during the simulation (trajectory) and by keeping the simulation conditions (*e.g.*

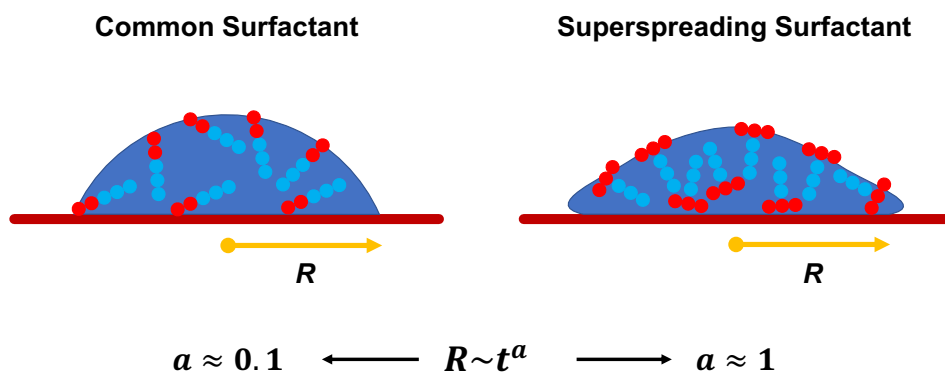


**Figure 2** Schematic illustration of aqueous droplets on a solid substrate at an intermediate time during spreading. Superspreading surfactants (right panel; common surfactants, left panel) cause the fast and complete spreading of droplets. The base radius of the droplet,  $R$ , changes with time,  $t$ , with a power law dependence described by the relation  $R \sim t^a$ , where  $a$  is the so-called spreading exponent. In the case of superspreading,  $a$  can obtain values as high as unity. Figure from Ref. R4.

thermodynamic parameters) under control. Moreover, the existence of a reliable force-field and sufficient computational resources was an essential element towards exploring the mechanism of superspreading and related factors that control the efficiency of droplet spreading [H1–H3].

In our case, the force-field was derived from the Statistical Associating Fluid Theory (SAFT), which is a molecular-based equation of state that can analytically describe experimental data [34,35]. In practice, the equation of state offers an accurate fit for the force-field parameters, where the key nonbonded interactions are described *via* the Mie potential. As a result, fluid–fluid and fluid–solid interactions (*e.g.* those between molecules of water, surfactant, and the substrate) are well reproduced by the force field, which includes various contributions (*e.g.* nonbonded terms) as outlined in SAFT [36–44]. In addition, the derived potentials between coarse-grained effective beads that represent distinct chemical groups of the molecules are transferable, which enables the simulation of systems consisting of different surfactant molecules. Still, the force-field parameters have to be derived for each functional group of atoms (effective bead) by the theory and reproduce the experimental data for each case (*e.g.* phase diagrams of pure components) [39], which has provided the basis for the agreement of the simulations with experiments [H1–H2].

In our case, a coarse-grained effective bead represented two water molecules, while other coarse-grained beads corresponded to siloxane ( $(\text{CH}_3)_3\text{Si-O}_{1/2}$  or  $\text{O}_{1/2}-\text{CH}_3-\text{Si-O}_{1/2}$ ) head moieties, as well as alkyl ether ( $-\text{CH}_2-\text{O}-\text{CH}_2-$ ) and alkane ( $-\text{CH}_2-\text{CH}_2-\text{CH}_2-$ ) chemical groups building the tail. Based on these beads, one can construct a large collection of superspreading and nonsuperspreading surfactants, which vary in their molecular composition and architecture, such as the ones presented in **Figures 3** and **4**. Also, the model takes into account the different masses of the groups represented by the effective beads. The SAFT model chooses the Mie potential for the interactions between chemical beads and assumes harmonic potentials for bonds and angles where necessary, for example, in the case of alkyl ether or alkane parts of the tail fragment. An implicit smooth and unstructured substrate was assumed by integrating the Mie potential over an implicit substrate of infinite thickness. The details of the force-field parameters have been reported in the discussed publications [H1–H3]. Further checks with experimental data at all stages of the model development were carried out to reproduce key properties of the system, such as the surface tension, the spreading behaviour, and observed effects of surfactant architecture and bilayer formation (**Figure 4**).

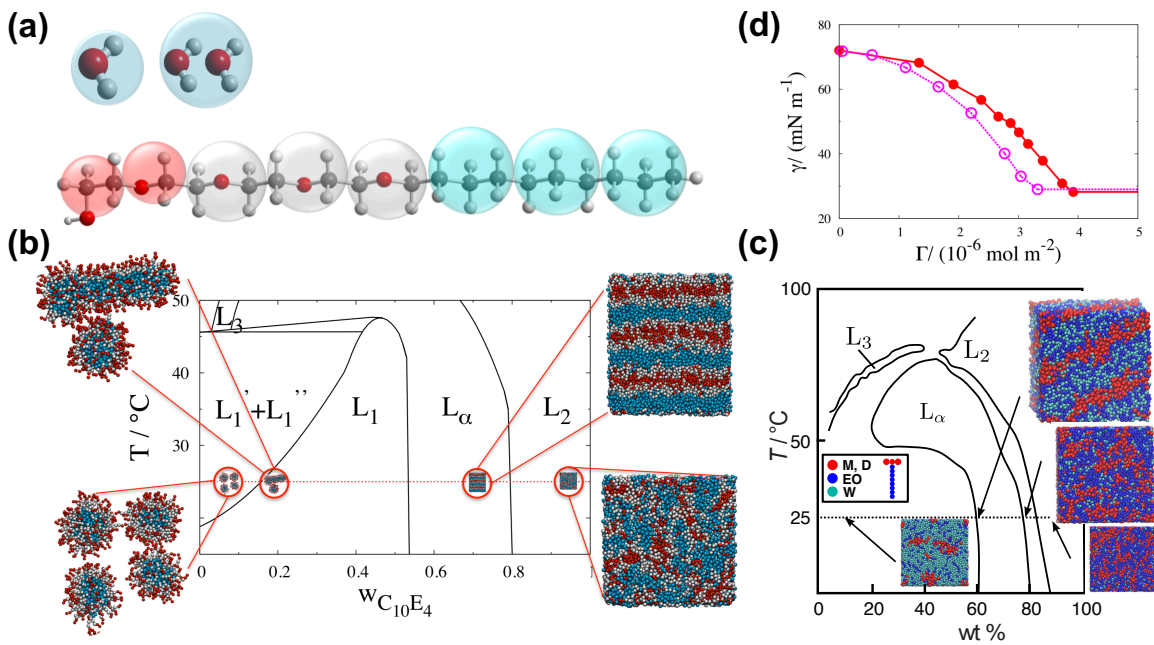


**Figure 3** (a) SAFT model for water (one-bead-one-water and one-bead-two-waters models) and the conventional (linear) C10E4 surfactant. Transparent spheres indicate the coarse-grained beads representing particular chemical moieties in the all-atom model. Alkane groups are in turquoise, ethoxyl groups in grey and red beads. From Ref. [38]. (b) Experimental phase diagram for C10E4 surfactant and representative snapshots from simulations based on the SAFT model. From Ref. [38]. (c) Experimental phase diagram for Silwet-L77 and representative snapshots from molecular dynamics simulations based on the SAFT model. From Ref. [H1]. (d) Surface tension,  $\gamma$ , versus surface excess concentration,  $\Gamma$ , in the case of C10E4 surfactant. Open symbols correspond to experimental data [45], while filled circles are results obtained by simulation based on the SAFT model from Ref. [38]. Figure from Ref. [R4].

The use of the SAFT coarse-grained force-field allowed us to simulate large droplets. The large size of the droplets was crucial to observe the key adsorption processes that constitute the superspreading mechanism. Droplets typically consisted of  $8 \times 10^4$  effective beads. In this case, each simulation for a droplet, which was able to completely spread, required as much as about two months on a K40 General Purpose Graphics Processing Unit (GPGPU). Coupled continuum and molecular dynamics simulations are particularly promising to reduce the computational burden to investigate such large droplets with surfactants. Although results of such an approach are published in Ref. [R3], they are not included in this Habilitation thesis.

Before discussing the main results of the molecular dynamics simulations, two considerations are essential: Scaling analysis for various properties (*e.g.* contact angle) has verified that properties of the system do not change as a function of the droplet size above a certain threshold. This threshold is about 65 000 effective beads and is model dependent [H1]. Also, in the case of surfactant-laden droplets it is important to consider the strong dependence of the *wt%* (percentage by weight) concentration on the droplet size, since *wt%* scales as  $1/R$ , where  $R$  is the radius of the droplet [H2]. This scaling of the concentration is more relevant in the case of nanodroplets, but it can also be to a certain extent present for millimetre-scale droplets, which may be partly the reason for inconsistencies that often occur among experimental data. In practice, the scaling simply means that the absolute value of the Critical Aggregation Concentration (CAC) in terms of *wt%* is different for droplets of different size. However, knowing the scaling ( $wt\% \sim 1/R$ ), we can always infer a fair comparison between droplets with different sizes, which is crucial in the case of nanodroplets. Moreover, this enabled the direct comparison with the experimental results in the literature when discussing the dependence of properties on surfactant concentration by using the CAC as a relative measure for surfactant concentration.

After setting the force-field parameters, the system setup needed to be defined, which consisted of an aqueous droplet laden with surfactant molecules and a smooth unstructured substrate (**Figure 4**). The consideration of this type of substrate puts the focus on the key processes of superspreading without risking the results being affected by the substrate structure, for example, avoiding pinning effects. Then, the molecular dynamics simulations were carried out in the canonical statistical ensemble at room temperature.

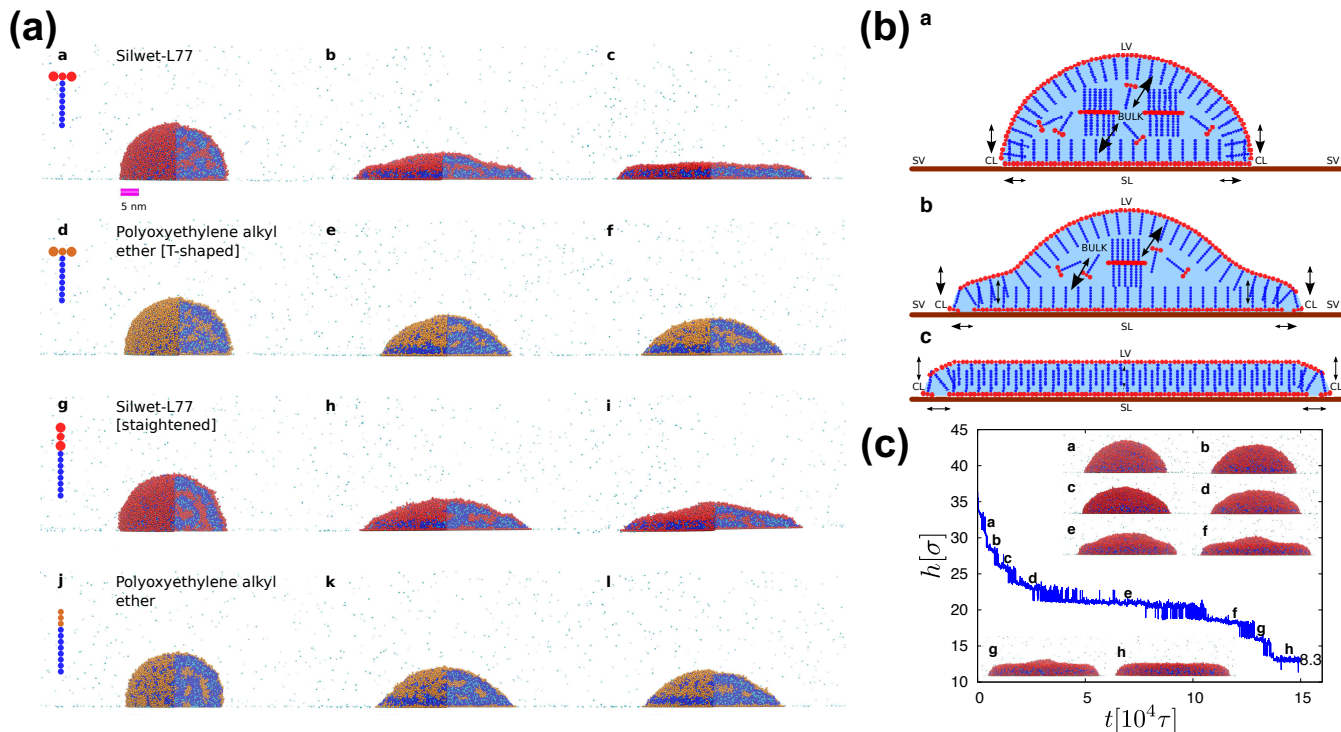


**Figure 4** Summary of main results obtained from the SAFT model on superspreading. **(a)** Time evolution of the spreading process for superspreading and nonsuperspreading surfactants, as indicated, at times (from left to right)  $0\tau$ ,  $7 \times 10^4\tau$ , and  $14 \times 10^4\tau$ , where  $\tau$  is the time unit. Hydrophobic beads are in orange or red and hydrophilic beads are in blue. Cyan beads represent water with each bead corresponding to two water molecules. From Ref. [H2]. **(b)** Schematic illustration of the leading adsorption processes during superspreading. The dominant direction of surfactant adsorption during spreading is illustrated with a larger arrow end. The essential processes for superspreading behaviour are the adsorption from the liquid–vapour (LV) interface onto the substrate through the contact line (CL) and the adsorption from the bulk to the LV interface. SL and SV indicate the solid–liquid and the solid–vapour interfaces, respectively. From Ref. [H1]. **(c)** The time evolution of the droplet height,  $h$ , during superspreading. Representative snapshots at each time are illustrated as indicated by letters a–h. In this case, the surfactant concentration is  $6.3 \times \text{CAC}$ . From Ref. [H1]. Figure from Ref. [R4].

The results are based on the ability of tracking the exact positions of the molecules and particularly the surfactants within the droplet at each time, which is a natural outcome of the molecular dynamics simulations. In this way, we could identify the key adsorption processes of the spreading mechanism, which are summarised in **Figure 4b**. Based on our simulations, we have identified that the first key process is the adsorption of surfactants from the liquid–vapour (LV) surface onto the substrate through the contact line (CL) [H2], in agreement with previous suggestions obtained by numerical simulation [5]. Moreover, we have found that superspreading surfactants have a larger probability of translocating through the contact line than common surfactants [H3]. In turn, this important adsorption process leads to a depletion of surfactant at the LV interface, as well as at the solid–liquid (SL) interface. For this reason, the first key process of the superspreading mechanism should be instantaneously followed by another process, that is the adsorption of surfactant from the bulk towards the interfaces (SL and LV, **Figure 4b**) [H1–H3]. This will result in the replenishment of these interfaces and the process will start over again until the droplet spreads completely reaching its final equilibrium state. In addition, we have found that a key feature of superspreading surfactants is their ability to quickly replenish the interfaces, which crucially depends on their lower aggregation tendency in comparison with nonsuperspreading

surfactants [H3]. This means that surfactants with larger hydrophobic attraction have a smaller tendency of replenishing the interfaces. A schematic picture of all adsorption processes during spreading is illustrated in **Figure 4b**.

Another success of the molecular simulations was the ability to capture the bilayer formation during superspreading and confirm its existence [H1–H3] (**Figure 4**), in agreement with experiments [22,46]. Moreover, by comparing different superspreading and conventional surfactants we have confirmed that the bilayer formation of the droplet is not a unique feature of superspreading [H2]. The influence of the molecular architecture on the spreading efficiency of the droplets was further investigated. To this end, a significant advantage of the simulation method with respect to experiments was the ability of changing easily the surfactant architecture. Based on the analysis of our results (**Figure 4a**), we have found that T-shape surfactants increase the spreading ability of the droplet despite the looser packing of this surfactant at the interfaces (LV and SL) *vis-a-vis* surfactants with linear architecture [H3]. When the chemistry of T-shape surfactant changed, adopting that of linear conventional surfactants, then the spreading deteriorated. Moreover, conventional surfactants of T-shape would perform better than linear conventional surfactants. In all cases, the spreading rate of common surfactants would be inferior with respect to superspreading surfactants (**Figure 4a**). We have also analysed various other properties of the systems based on a wide selection of superspreading and nonsuperspreading surfactants. In general, a smaller chain length of surfactants will lead to faster diffusion and smaller contact angles of the droplet. By characterising a number of properties that can influence superspreading, the obtained results have revealed that apart from the surfactant chemistry, all other properties (*e.g.* molecular architecture) have a minor effect on the spreading ability of surfactant-laden droplets [H3].

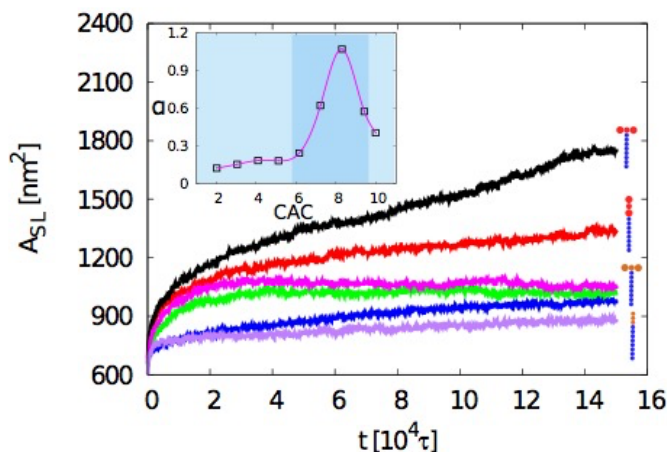


**Figure 5** Area of the droplet vs time for the surfactants of **Figure 4**. Inset shows the characteristic peak of the spreading rate exponent vs concentration for the Silwet-L77 surfactant, where the superspreading regime concentration is highlighted with darker colour. From Ref. [H2].

One more important success of the SAFT model was the ability to reproduce the characteristic experimental peak of the spreading exponent as a function of surfactant concentration (**Figure 5**). That is, the increase of surfactant concentration initially favours spreading, while further increase leads to less efficient spreading. This is characteristic of the superspreading surfactants and values as high as unity have been reported for specific concentrations [H2]. Moreover, simulations have been able to provide the reasons for which exceedingly high concentration of surfactant leads to deteriorating efficiency of spreading. This is due to a combined effect of reduced bulk diffusion and interface replenishment, which is affected by the aggregation tendency of surfactant [H3]. For conventional nonionic surfactants, the slow replenishment of interfaces with surfactant from the bulk is the reason for nonsuperspreading behaviour,

which has been linked to the higher aggregation tendency of these surfactants [H3].

In summary, molecular dynamics simulations based on the SAFT coarse-grained force-field have been able to elucidate the superspreading mechanism and the influence of key factors that dictate this phenomenon. Based on the results of our simulations, design principles for superspreading surfactants have been proposed and the role of different properties in the superspreading process have been identified and discussed. Those concepts and results that stem from the above studies have been discussed in greater detail in publications H1–H3 along with many technical details on the developed model and the analysis of the results. Possible strategies for linking molecular and continuum simulations together with preliminary results underlining the parameters that can be passed between molecular dynamics and computational fluid dynamics engines can be found in [R3]. This work holds great promise for further research in the future towards novel

multiscale modelling methods, which have the potential of becoming wider applicable. A by-product of our research tasks has also been an accurate way of measuring the contact angle based on the curvature of the droplet [H1]. The molecular dynamics simulations of the superspreading phenomenon have been reviewed in [R4] as an invited article in a special issue in *Fluids*. Our research has also been featured on the covers of *Soft Matter* [H2] and *Langmuir* [R3] journals.

### 5.3.2 Durotaxis (H4)

A range of technologies require the ability to steer the motion of nanodroplets on solid substrates, such as nanoscale actuation and energy conversion [7,11,47–52]. This can be done by exploiting a gradient of a certain property along the substrates, for example, surface chemistries with different patterns [53–55], temperature and electric potential gradients [48,56], and surface topography [57–61]. In the case of durotaxis, a nano-object (*e.g.* nanodroplet) can move on a solid substrate without an energy source due to a stiffness gradient along the substrate. Apart from its relevance for applications, recent studies have also shown that cell motion can be guided by substrate rigidity and that this phenomenon shares similarities with the stiffness-guided motion of droplets on solid substrates [62]. It is believed that weak van der Waals interactions are responsible for both the motion in the case of the cells and in the case of the droplets [11,63]. In this Habilitation thesis, the driving force of durotaxial motion and the role of parameters affecting durotaxis in the case of a nanodroplet on a solid substrate has been identified [H4]. To achieve this objective, large-scale canonical-ensemble molecular-dynamics simulations based on a coarse-grained force-field were employed.

As illustrated in **Figure 6**, the system consists of a droplet with  $N_p$  number of polymer chains of length  $N$  each and a substrate with a stiffness gradient along the  $x$  direction. The force-field was based on the well-known bead-spring model [64], where all coarse-grained beads interact *via* the *Lennard-Jones* potential, while beads were linked by using the finitely extensible nonlinear elastic (FENE) potential to form the polymer chains. In this way, we could vary the length of the polymer chains,  $N$ , which was used to tune the viscosity of the droplet. The substrate consisted of a single layer of beads, where in the  $x$  direction a stiffness gradient was applied by varying the force constant of a harmonic potential that kept the substrate beads at their equilibrium positions (**Figure 6 middle panel**). The exact parameters and other technical details of the model can be found in Ref. [H4].

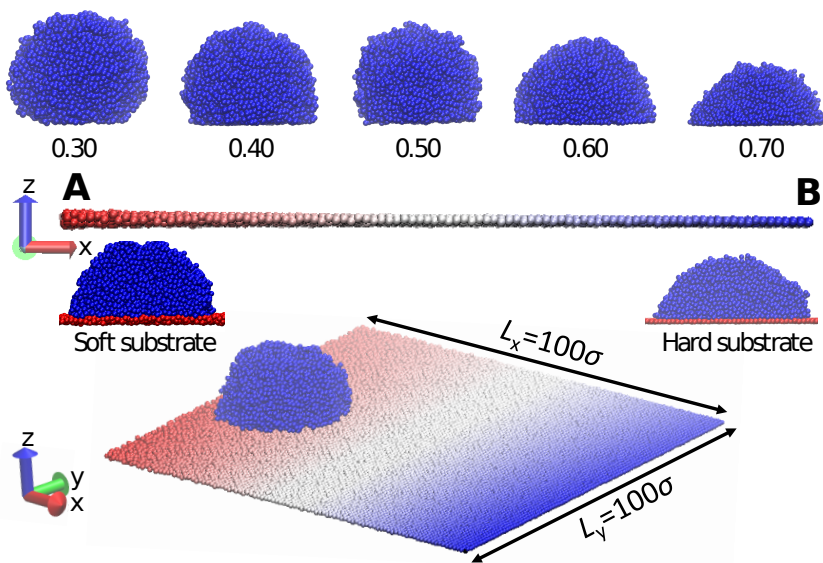


**Figure 6 Upper panel:** The shape of the droplet on a stiff substrate for different strengths of attraction between the droplet and the substrate (LJ parameter  $\epsilon_{sp} = 0.3-0.7$  is the range of values for the *Lennard-Jones* potential depth for the interaction between the substrate and the droplet beads). **Middle panel:** The effect of the substrate stiffness gradient in the  $x$  direction marked in red (left side of the substrate, A) for the soft parts of the substrate and in blue (on the B-side of the substrate in the  $x$  direction) indicating the highest rigidity. Two examples of droplets 'sitting' on a soft and a stiff substrate with the same attraction potential between the droplet and the substrate are illustrated as indicated. **Bottom panel:** A typical setup of an initial configuration for a molecular dynamics simulation of a droplet on a substrate. The colour gradient indicates the change in the degree of stiffness in the  $x$  direction. From Ref. [H4].

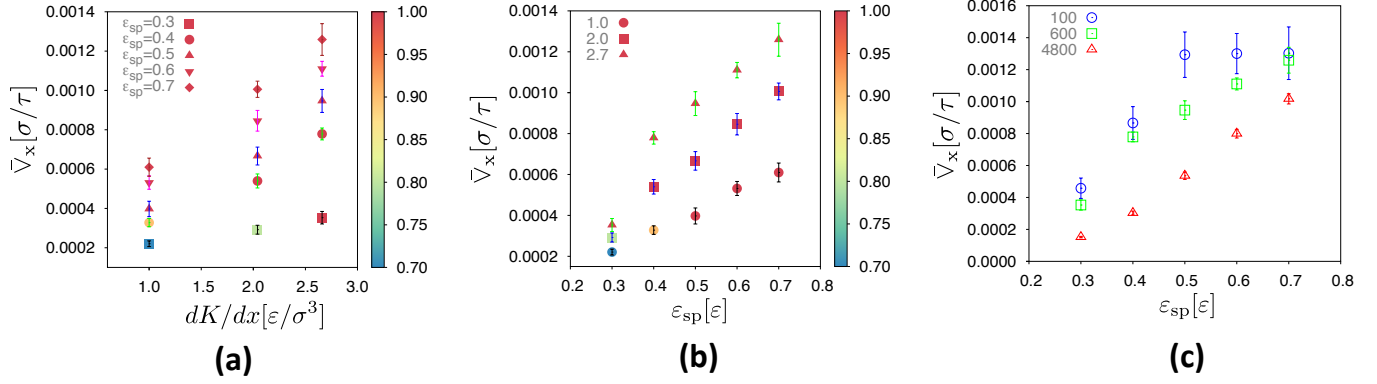


**Figure 7** (a) Mean droplet velocity *versus* stiffness gradient for various levels of attraction (LJ parameter  $\epsilon_{sp} = 0.3\text{--}0.7$ ) between the droplet and the substrate. The colour bar indicates the probability of durotaxis (reaching point B from point A, **Figure 6 middle panel**) within the available simulation time. The droplet is formed by 600 chains with 10 beads each. (b) Same as in (a), but the mean velocity of translocation during durotaxis is plotted *versus* the attraction strength ( $\epsilon_{sp}$ ) between the droplet and the substrate for different stiffness gradients, as indicated. (c) Mean droplet-velocity dependence *versus* the droplet–substrate attraction strength for droplets of different sizes (the number of polymer chains is 100, 600, and 4800, as indicated, with each polymer chain containing 10 beads). From Ref. [H4].

The direction of the durotaxial motion, whether it is from the softer to the stiffer areas or in the opposite direction was largely controversial and it was one of the key questions that was addressed. While in the case of soft substrates it has been shown that the droplet moves from the stiffer to the softer regions [7], in the case of solid (hard) substrates durotaxial motion takes place towards areas with larger rigidity [11]. Our results confirmed that in the case of nanodroplets on solid substrates, the motion is towards the stiffer regions (from A to B, *cf.* **Figure 6**), similarly to the durotaxis of cells on biological tissues [62]. Moreover, simulations have elucidated various parameters that influence the efficiency of durotaxis based on the average droplet velocity of translocation from one side of the substrate (softer regions) to the other side (more rigid regions). It has been revealed that the durotaxial motion becomes more efficient, when: the stiffness gradient is larger (**Figure 7a**), the attraction between the droplet and the substrate is larger (**Figure 7b**), the size of the droplet is smaller (**Figure 7c**) and the viscosity of the droplet is smaller (**Figure 8**). Also, the viscosity plays a greater role in the case of larger droplets. Finally, it was found that there is a threshold value for the efficiency of the durotaxial motion, which has been identified in the case of small droplets (**Figure 7c**). Thus, the study of Ref. [H4] has fully elucidated the effect of key factors that determine the efficiency of durotaxis.

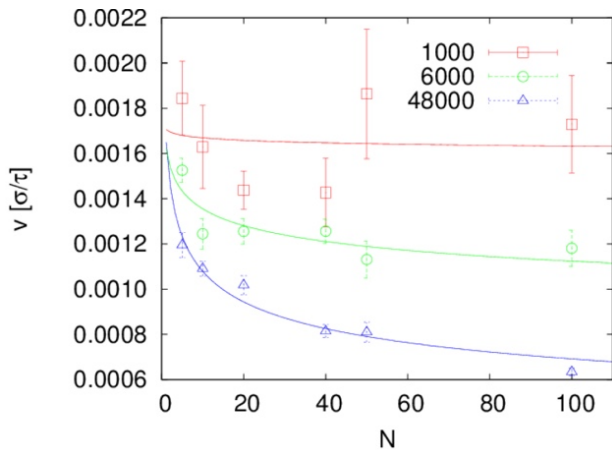


**Figure 8** Dependence of the mean durotaxial velocity ( $v$ ) on the chain length,  $N$ , for different droplet sizes (total number of beads: 1000, 6000, 48000), as indicated. Note that  $N \sim$  viscosity. Unpublished data.

A key result of the molecular dynamics simulations has been the identification of the driving force that leads to the durotaxis motion of the nanodroplet, which could not be identified by experiment, theory, or continuum simulation because this would require access to the molecular detail of the interactions at the solid–liquid interface between the substrate and the droplet. By conducting a careful analysis of the different energy contributions during durotaxis, it has been concluded that the minimisation of the system energy is the main trigger of durotaxis. In particular, the main contribution comes from the energy reduction at the solid–liquid interface between the droplet and the substrate (**Figure 9**). As the droplet moves to stiffer areas, it establishes a larger number of contacts with the substrate, what leads to a smaller interfacial energy. Further

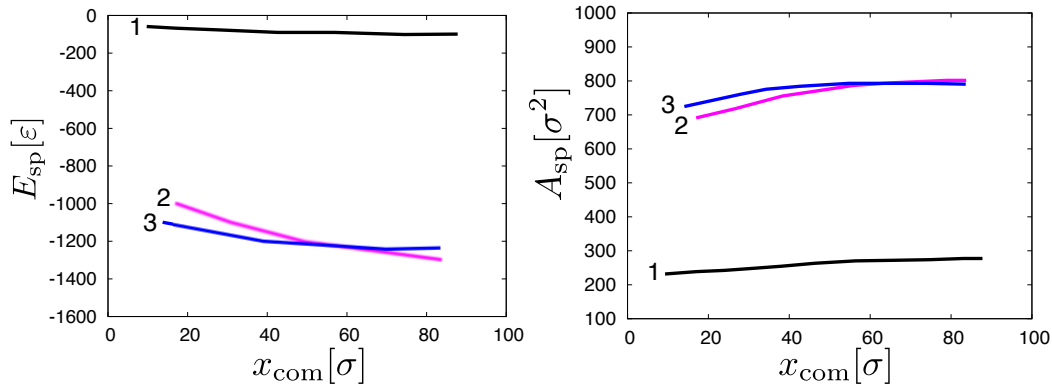


**Figure 9** The interfacial energy between the nanodroplet and the substrate (**left panel**) and the interfacial area (**right panel**) as a function of the centre-of-mass-position (com) of the droplet for three different study cases 1, 2, and 3, as indicated. In the case of optimal durotaxis (2, 3), the energy drops as the droplet moves to stiffer parts of the substrate. In contrast, when this energy drop is negligible, the durotaxis motion does not take place (1). It has been found that the gradient of the solid–liquid interfacial energy is the driving force of durotaxis. From Ref. [H4].

analysis has shown that the efficiency of the durotaxis motion actually depends on the gradient of the interfacial energy, which is the driving force of this phenomenon. Moreover, as the droplet forms a larger number of contacts with the substrate during durotaxis, the contact angle decreases (**Figure 10**). Furthermore, as a result of the simulations, it has been revealed that the contact angle decreases when the stiffness of the substrate is higher. By monitoring the velocities of each bead at different times during durotaxis, it has been concluded that there is no particular pattern of particle velocities that have been identified in the case of other *in silico* experiments with droplets (*e.g.* carpet motion). In fact, the droplet moves back and forth during durotaxis due to the thermal fluctuations with the stiffness gradient determining the direction of the durotaxis motion, that is from softer to more rigid areas of the substrate.

In summary, this work has clarified the mechanism of durotaxis in the context of a nanodroplet on a solid substrate by identifying the gradient of the interfacial energy as the driving force of this phenomenon. Moreover, simulations have elucidated the role of key parameters affecting the efficiency of durotaxis. Thus, important insights into the mechanisms of nanoscale motion have been provided, which have direct implications for applications in nanofluidics, microfabrication and coating design, as well as biology and medicine.

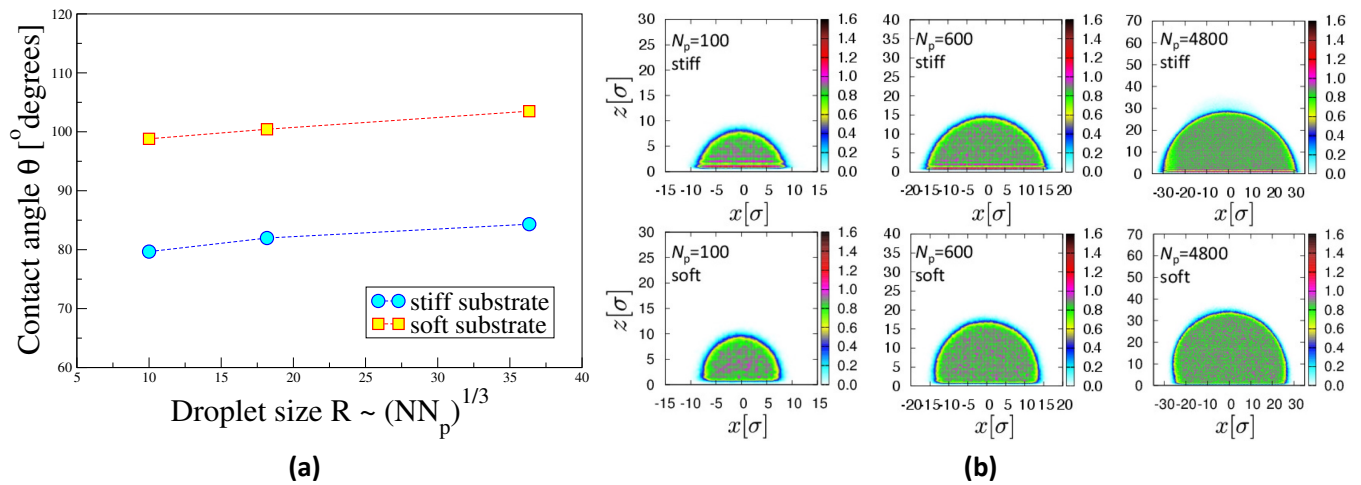


**Figure 10 (a)** Variation of the contact angle,  $\theta$ , of sessile nanodrops with drop radius ( $R$ ) on a soft and stiff substrate, as indicated.  $N$  is the chain length and  $N_p$  the number of polymer chains in the droplet. **(b)** Density profiles on the  $x$ – $z$  plane (droplet cross-section) for different droplet sizes ( $N_p$ ) and substrate stiffness as indicated. From Ref. [H4].

### 5.3.3 Surface Nanobubbles (H5)

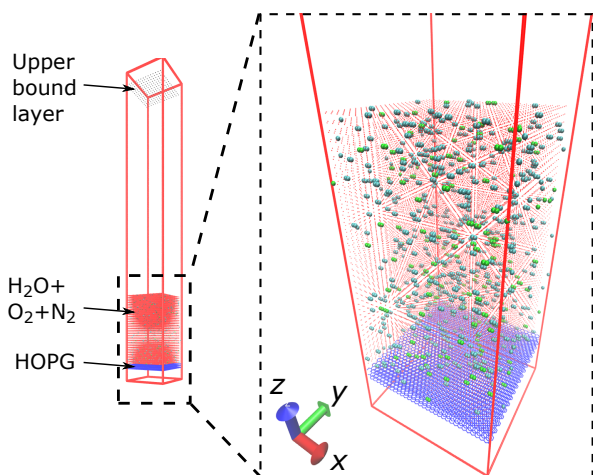


**Figure 11** Perspective view of a typical initial configuration of the system used in the simulations investigating the subsequent formation and dissolution of surface nanobubbles on an HOPG substrate immersed in water. The magnified region highlights the gas molecules (cyan colour for N<sub>2</sub> and green colour for O<sub>2</sub>) dispersed randomly within the aqueous medium (in red). The HOPG substrate (in blue) at the bottom of the simulation box consists of three layers of carbon atoms arranged on a hexagonal lattice. From Ref. [H5].

Surface nanobubbles are gaseous domains at the interface between liquids and solid substrates. Although their existence was speculated earlier by Parker *et al.* [65], Lou *et al.* [66] provided the first AFM image of hour-long stable nanobubbles on a mica substrate immersed in water about 20 years ago. While the theoretical expectation (Rayleigh–Plesset theory) is that surface nanobubbles shall dissolve immediately due to the high Laplace pressure ( $\Delta p = 2\gamma/R$ , where  $\gamma$  is the surface tension and  $R$  the bubble radius) [67], these nano-objects can remain stable for hours or even days, as for example in the case of nanobubbles on a highly oriented pyrolytic graphite (HOPG) [68,69]. Owing to their high stability and spontaneous formation on surfaces, nanobubbles play an important role in many modern applications, such as separation, flotation and drag reduction processes, as well as in nanocomposite foams, catalysis and electrolysis and transport in nanofluidic devices, *etc.* [12–19]. In this context, theory, simulation, and experiment have attempted to describe the mechanisms of nanobubbles formation and dissolution, in this way attempting to explain their high stability. Moreover, fundamental properties of surface nanobubbles, such as their density, had remained unknown despite intensive research over the last two decades. Addressing

these questions was the aim of our molecular dynamics study of surface nanobubbles in Ref. [H5], which offers significant advantages over theory and experiment by providing the molecular-level resolution required to describe the relevant underlying processes.

In Ref. [H5], an all-atom model was adopted, representing the water molecules with the SPC/E force-field, the nitrogen and oxygen molecules with the TraPPE force-field, while an all-atom force-field was tuned for the HOPG substrate carbon atoms in order to reproduce the correct contact angle of a pure water droplet on the HOPG substrate. The initial setup of the studied system is presented in **Figure 11**. By means of our molecular dynamics simulations in the canonical ensemble, it has been found that the formation of nanobubbles is driven by a nucleation process. The gas molecules (N<sub>2</sub> and O<sub>2</sub>) were initially distributed in water and they gradually formed clusters, which later grew with the addition of

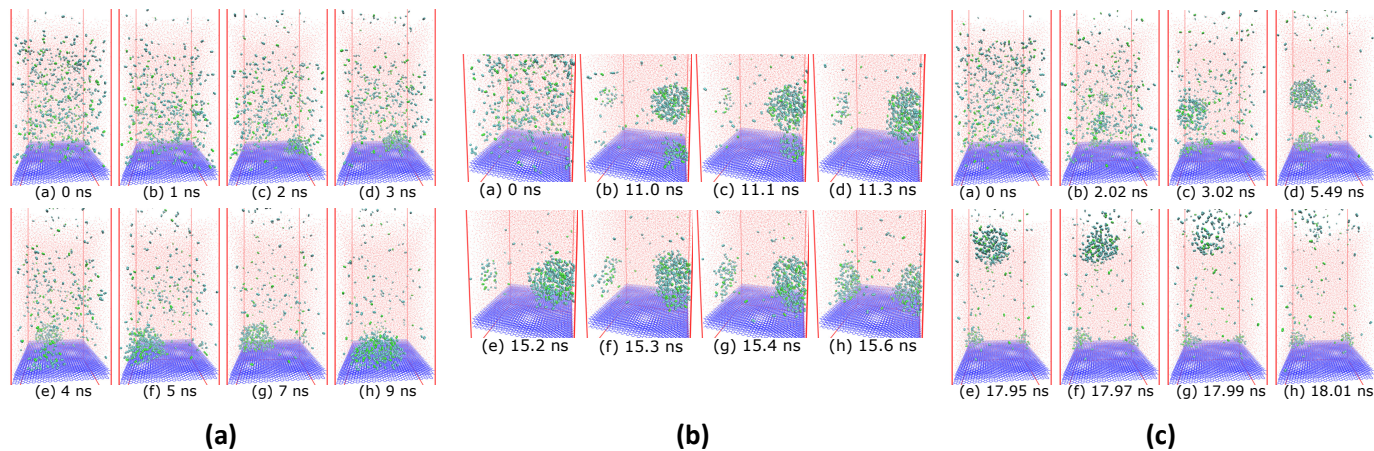


**Figure 12** Different scenarios of nanobubbles formation. **(a) Formation** of a surface nanobubble on an HOPG substrate at different times as indicated. **(b) Coalescence** of two nanobubbles to form a larger bubble and its subsequent spreading on the HOPG substrate illustrated with snapshots at different times as indicated. **(c) Pop** of a nanobubble towards the top water–air surface illustrated with snapshots at different times as indicated. From Ref. [H5].

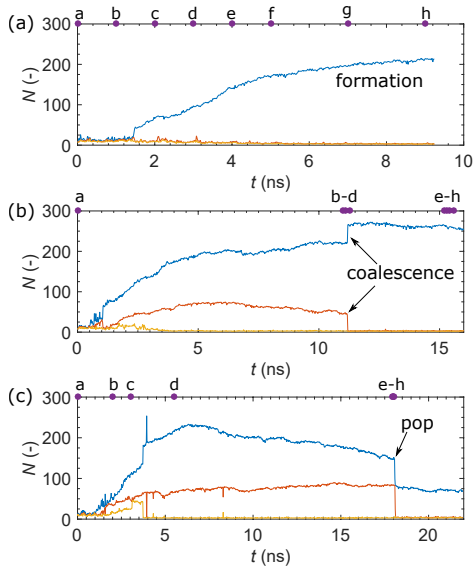


**Figure 13** The time evolution of the three largest clusters of air molecules for each of the cases of Figure 12 (**formation**, **coalescence**, **pop**) with the small letters on the axis of the plots corresponding to the indicators of snapshots at different times in Figure 12. From Ref. [H5].

would dissolve with the same rate. The simulations have also indicated that the presence of the substrate offers a greater stability to the nanobubble, but it is not sufficient to maintain this stability of nanobubbles for exceedingly large times. This means that a longer lifetime of nanobubbles may be attributed to pinning of the contact line (e.g. due to substrate defects), what is in line with the current literature [R1].

**Figure 14** summarises various properties of surface nanobubbles. It has been found that nanobubbles are much denser than a typical gas phase, with values of density closer to that being typical for liquids. A detailed analysis revealed that the actual distance between gas molecules in the nanobubble is in the range of the *van der Waals* interactions, which indicates that air molecules are condensed in the nanobubble phase. As a result, air molecules inside the surface nanobubbles are dominated by the potential instead of the kinetic energy, which enhanced the stability. Previous

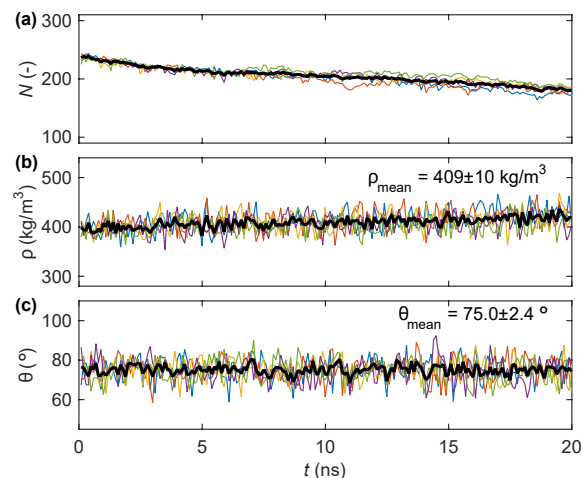


**Figure 14** Properties of surface nanobubbles on HOPG substrates as a function of time. **(a)** Size of nanobubbles,  $N$ , in terms of the number of molecules ( $N$ ); bubbles become smaller as air molecules dissolve in water; **(b)** density,  $\rho$ , of nanobubbles, and **(c)** contact angle,  $\theta$ , of nanobubbles. From Ref. [H5].

nearby gas molecules (**Figure 12**). This is due to the oversaturation of gas in water, which favours the formation of gas phases of different properties (*i.e.* different composition of  $\text{N}_2$  and  $\text{O}_2$ ). The favourable interactions between gas molecules as well as between gas molecules and the substrate in comparison with the gas–water interactions, led to the formation of nanobubbles on the HOPG substrate, which is energetically the most favourable position for the gas molecules in the liquid phase (**Figure 12a**). The formation of nanobubbles may also include the coalescence of nanobubbles, which may end up on the HOPG substrate or pop up at the liquid–air interface (**Figures 12b** and **12c**, respectively). The size of the nanobubbles during their formation in the above scenarios, shown in **Figure 12**, are plotted *versus* time in **Figure 13**. Overall, nanobubbles on the HOPG substrate remain stable, which underlines the role of the substrate in the stability of surface nanobubbles. It has also been found that the formation process depends on the degree of saturation of the system, where air molecules can collectively and diffusively reach the HOPG substrate. Then, the formed nanobubbles dissolve at a rate that depends on the maximum size of the nanobubble. The dissolution process is noncollective, since the size of the nanobubble smoothly decreases (**Figure 14a**). It has been found that nanobubbles with the same size

experiments could only confirm that surface nanobubbles entirely consist of air molecules. Our studies provided for the first time an estimate of the air density in the nanobubbles, which has been validated by recent experimental data [70]. Moreover, the contact angle in the case of surface nanobubbles was different than that in the respective nanodroplet. In particular, the nanobubble contact angle is about  $10^\circ$  larger than the nanodroplet contact angle, which is in agreement with previous experimental findings [71]. This has indicated that the contact angle is not only a property of the substrate, but it also depends on the configuration of the system (*e.g.* the ratio of water to air molecules). Finally, we have measured the surface tension of the nanobubbles, which has been found about 10% smaller than the surface tension for a typical water–air interface at atmospheric conditions. This indicates the strong effect of the gas phase and the higher density of the gas phase, due to the higher net force produced by the greater attraction between water

and air molecules. That is, a higher air density can reduce the energetic penalty for the formation of the air–water interface.

This research has demonstrated the possibility of addressing key questions for surface nanobubbles by using molecular dynamics simulation of atomistic force-fields. The above investigations have provided insights into the formation and dissolution mechanisms of nanobubbles and accurate predictions of main properties for these gaseous phases on HOPG substrates, which are in agreement with experimental measurements. Hence, the obtained results have important implications for many relevant phenomena in nature, such as nucleation in boiling and cavitation processes, where nanobubbles can act as nucleation sites [72]. Further applications of these results include areas of materials synthesis, micro- and nanofluidics as well as advanced diagnostics and drug delivery. These results have been discussed with other important advances in the area of surface nanobubbles in a recent special-issue review article [R1].

#### 5.3.4 Summary of the significance of publications H1–H5

The above studies have focused on addressing important questions regarding interfacial phenomena involving nanobubbles and nanodroplets in contact with solid substrates. To tackle these objectives, the advantages of the molecular dynamics methodology have been exploited. Due to its molecular-scale resolution, molecular dynamics simulation enabled the tracking of particles and their velocities at any time during the *in silico* experiments, which allowed us to monitor the molecular mechanisms of the underlying physical processes and provide accurate estimates of relevant properties of the studied interfacial phenomena.

The first research theme dealt with the superspreading phenomenon [H1–H3]. The main adsorption processes of the superspreading mechanism have been identified, namely the direct adsorption of surfactant through the contact line and the fast replenishment of the interfaces with surfactant from the bulk. The SAFT model has been able to reproduce the characteristic peak for the spreading exponent as a function of the surfactant concentration, the characteristic bilayer formation, and finally elucidate the role of various factors on superspreading. Moreover, T-shape surfactants have been found to be better spreaders, but the most important element of superspreading surfactants is their chemical composition rather than its molecular architecture. The intrinsic aggregation tendency of surfactants is crucial and affects their ability to quickly replenish the droplet interfaces. Finally, guidelines for surfactant designs for applications that require efficient spreading have been suggested, such as technologies for coating and herbicides production, and enhanced oil recovery.

The study on the durotaxis of a liquid droplet on a solid substrate has also provided concrete outcomes [H4]. It has been revealed that the droplet motion takes place along the direction of the stiffness gradient, that is from softer areas towards stiffer areas of the substrate. Moreover, a smaller size of the droplet, a lower viscosity, a greater attraction to the substrate, and a greater stiffness gradient, are factors that favour the durotaxis motion. Finally, it has been concluded that the driving force of durotaxis is the gradient of the interfacial energy between the droplet and the substrate. The elucidation of these effects has significant implications for applications that require the guided motion of droplets by interfacial interactions in nanofluidics and microfabrication, as well as coating technology, biotechnology and medicine.

In the theme of surface nanobubbles on solid substrates two main objectives have been achieved [H5]. Firstly, the key mechanisms of the formation and the dissolution of surface nanobubbles have been unravelled. Secondly, accurate estimates of their main properties (*e.g.* density, contact angle, surface tension) have been provided. Thus, it is anticipated that this work shall impact our understanding in applications of surface nanobubbles in materials synthesis, micro- and nano-fluidics, as well as advanced diagnostics and drug delivery.

## Publications related to the Habilitation thesis

**R1. P. E. Theodorakis**, Z. Che, “Surface nanobubbles: Theory, Simulation, and Experiment. A review”, *Advances in Colloid and Interface Science* 272, 101995 (2019)

**R2. P. E. Theodorakis**, E. A. Müller, R. V. Craster, O. K. Matar, “Insights into surfactant-assisted superspreading”, *Current Opinion in Colloid and Interface Science* 19, 283 (2014)

**R3. E. R. Smith, P. E. Theodorakis**, R. V. Craster, O. K. Matar, “Moving contact lines: linking molecular dynamics and continuum-scale modelling”, *Langmuir* 34, 12501 (2018)

**R4. P. E. Theodorakis**, E. R. Smith, R. V. Craster, E. A. Müller, O. K. Matar “Molecular dynamics simulation of the superspreading of surfactant-laden droplets. A review”, *Fluids* 4, 176 (2019)

## 5.3.5 References

- [1] A. Nikolov, D. Wasan, *Curr. Opin. Colloid Interface Sci.* 3, 247 (1998)
- [2] L. Bocquet, E. Charlaix, *Chem. Soc. Rev.* 39, 1073 (2010)
- [3] J. Luo, J.-H. Im, M.T. Mayer, M. Schreier, M.K. Nazeeruddin, N.-G. Park, S.D. Tilley, H.J. Fan, M. Grätzel, *Science* 345, 1593 (2014)
- [4] T. Stoebe, Z. Lin, R.M. Hill, M.D. Ward, H.T. Davis, *Langmuir* 12, 337 (1996)
- [5] G. Karapetsas, R.V. Craster, O.K. Matar, *J. Fluid Mech.* 670, 5 (2011)
- [6] D. Lohse, X. Zhang, *Rev. Mod. Phys.* 87, 981 (2015)
- [7] R.W. Style, Y. Che, S.J. Park, B.M. Weon, J.H. Je, C. Hyland, G.K. German, M.P. Power, L.A. Wilen, J.S. Wettlaufer, E.R. Dufrense, *Proc. Natl. Acad. Sci. U.S.A.* 110, 12541 (2013)
- [8] J. Venzmer, *Curr. Opin. Colloid Interface Sci.* 16, 335 (2011)
- [9] E.G. Schwarz, W.G. Reid, *Ind. Eng. Chem.* 56, 26 (1964)
- [10] C.-M. Lo, H.-B. Wang, M. Dembo, Y.-L. Wang, *Biophys. J.* 79, 144 (2000)
- [11] T. Chang, H. Zhang, Z. Guo, X. Guo, H. Gao, *Phys. Rev. Lett.* 114, 015504 (2015)
- [12] S. Calgaroto, K. Wilberg, J. Rubio, *Miner. Eng.* 60, 33 (2014)
- [13] L. Chen, D. Rende, L.S. Schadler, R. Ozisik, *J. Mater. Chem. A* 1, 3837 (2013)
- [14] S. Liu, J. DuVigneau, G.J. Vansco, *Eur. Polym. J.* 65, 33 (2015)
- [15] E. Lukianova-Hleb, Y. Hu, L. Latterini, L. Tarpani, S. Lee, R.A. Drezek, J.H. Hafner, D.O. Lapotko, *ACS Nano* 4, 2109 (2010)
- [16] J. Zou, H. Zhang, Z. Guo, Y. Liu, J. Wei, Y. Huang, X. Zhang, *Langmuir* 34, 14096 (2018)
- [17] F. Hui, B. Li, P. He, J. Hu, Y. Fang, *Electrochem. Commun.* 11, 639 (2009)
- [18] D. Lohse, *Phys. Rev. Fluids* 3, 110504 (2018)
- [19] I. Kumagai, Y. Takahashi, Y. Murai, *Ocean Eng.* 95, 183 (2015)
- [20] A. Sankaran, S.I. Krakashev, S. Soumyadip, N. Grozev, A.L. Yarin, *Adv. Colloid Interface Sci.* 263, 1 (2019)
- [21] N.M. Kovalchuk, A. Trybala, O. Arjmandi-Tash, V. Starov, *Adv. Colloid Interface Sci.* 233, 155 (2016)
- [22] R.M. Hill, *Curr. Opin. Colloid Interface Sci.* 3, 247 (1998)
- [23] J. Radulovic, K. Sefiane, E.R. Shanahan, *J. Phys. Chem. C* 114, 13620 (2010)
- [24] [29] S. Semenov, A. Trybala, H. Agogo, N. Kovalchuk, F. Ortega, R.G. Rubio, V.M. Starov, M.G. Velarde, *Langmuir* 29, 10028 (2013)
- [25] N.A. Ivanova, Z.B. Zhantenova, V.M. Starov, *Colloids Surf. A* 413, 307 (2012)
- [26] J. Radulovic, K. Sefiane, M.E. Shanahan, *J. Colloid Interface Sci.* 332, 497 (2009)
- [27] N. Ivanova, V. Starov, R. Rubio, H. Ritacco, N. Hilal, D. Johnson, *Colloids Surf. A* 354, 143 (2010)
- [28] T. Svitova, R.M. Hill, Y. Smirnova, A. Stuermer, G. Yakubov, *Langmuir* 14, 5023 (1998)
- [29] J. Radulovic, K. Sefiane, M.E.R. Shanahan, *Chem. Eng. Sci.* 65, 5251 (2010)
- [30] M.J. Rosen, Y. Wu, *Langmuir* 17, 7296 (2001)
- [31] M.J. Rosen, Y. Wu, *Langmuir* 18, 2205 (2002)

- [32] J. Radulovic, K. Sefiane, M.E.R. Shanahan, *J. Bionic Eng.* 6, 341 (2009)
- [33] N.A. Ivanova, V.M. Starov, *Curr. Opin. Colloid Interface Sci.* 16, 285 (2011)
- [34] V. Papaioannou, T. Lafitte, C. Avendaño, C.S. Adjiman, G. Jackson, E.A. Müller, A. Galindo, *J. Chem. Phys.* 140, 054107 (2014)
- [35] T. Lafitte, A. Apostolakou, C. Avendaño, A. Galindo, C.S. Adjiman, E.A. Müller, G. Jackson, *J. Chem. Phys.* 139, 154504 (2013)
- [36] C. Herdes, E.E. Santis, C. James, J. Eastoe, E.A. Müller, *J. Colloid Interface Sci.* 445, 16 (2015)
- [37] O. Lobanova, A. Mejía, G. Jackson, E.A. Müller, *J. Chem. Thermodyn.* 93, 320 (2016)
- [38] O. Lobanova, ‘Development of coarse-grained force fields from a molecular based equation of state for thermodynamic and structural properties of complex fluids’, Ph.D. Thesis, *Imperial College London*, UK (2014)
- [39] E.A. Müller, G. Jackson, *Annu. Rev. Chem. Biomol. Eng.* 5, 405 (2014)
- [40] O. Lobanova, C. Avendaño, T. Lafitte, E.A. Müller, G. Jackson, *Mol. Phys.* 113, 1228 (2015)
- [41] C. Avendaño, T. Lafitte, A. Galindo, C.S. Adjiman, G. Jackson, E.A. Müller, *J. Phys. Chem. B* 115, 11154 (2011)
- [42] C. Avendaño, T. Lafitte, A. Galindo, C.S. Adjiman, E.A. Müller, G. Jackson, *J. Phys. Chem. B* 117, 2717 (2013)
- [43] G. Jiménez-Serranos, C. Hermes, A.J. Haslam, G. Jackson, E.A. Müller, *Macromolecules* 50, 4840 (2017)
- [44] C. Herdes, A. Ervik, A. Mejía, E.A. Müller, *Fluid Phase Equilib.* 476, 9 (2017)
- [45] J. Eastoe, J.S. Dalton, P.G.A. Rogueda, E.R. Crooks, A.R. Pitt, E.A. Sinister, *J. Colloid Interface Sci.* 188, 423 (1997)
- [46] E. Ruckenstein, *J. Colloid Interface Sci.* 179, 136 (1996)
- [47] M. Srinivasarao, D. Collings, A. Philips, S. Patel, *Science* 292, 79 (2001)
- [48] M.K. Chaudhury, G.M. Whitesides, *Science* 256, 1539 (1992)
- [49] T.-S. Wong, S.H. Kang, S.K.Y. Tang, E.J. Smythe, B.D. Hatton, A. Grinthal, J. Aizenberg, *Nature* 477, 443 (2011)
- [50] J.T. Pham, L. Xue, A. Del Campo, M. Salierno, *Acta Biomater.* 38, 106 (2016)
- [51] K.A. Lazopoulos, D. Stamenovic, *J. Biotech.* 41, 1289 (2008)
- [52] M. Becton, X. Wang, *RSC Adv.* 6, 51205 (2016)
- [53] H. Gau, S. Herminghaus, P. Lenz, R. Lipowsky, *Science* 283, 46 (1999)
- [54] H. Siringhaus, T. Kawase, R.H. Friend, T. Shinoda, M. Inbasekaran, W. Wu, E.P. Woo, *Science* 290, 2123 (2015)
- [55] P.Z. Hanakata, B.A. Pazmiño Betancourt, J.F. Douglas, F.W. Starr, *J. Chem. Phys.* 142, 234907 (2015)
- [56] A. Darhuber, S. Troian, *Annu. Rev. Fluid Mech.* 37, 425 (2005)
- [57] A. Lafuma, D. Quéré, *Nat. Mater.* 2, 457 (2003)
- [58] L. Courbin, E. Denial, E. Dressaire, M. Roper, A. Ajdari, H.A. Stone, *Nat. Mater.* 6, 661 (2007)
- [59] N. Tretyakov, M. Müller, *Soft Matter* 10, 4373 (2014)
- [60] N. Tretyakov, M. Müller, *Soft Matter* 9, 3613 (2013)
- [61] G. Karapetsas, N.T. Chamakos, A.G. Papathanasiou, *J. Phys.: Condens. Matter* 28, 085101 (2016)
- [62] C.-M. Lo, H.-B. Wang, M. Dembo, Y.-L. Wang, *Biophys. J.* 79, 144 (2000)
- [63] A.S. Barnard, *Nature* 519, 37 (2015)
- [64] K. Kremer, G.S. Grest, *J. Chem. Phys.* 92, 5057 (1990)
- [65] J.L. Parker, P.M. Claesson, P. Attard, *J. Phys. Chem.* 98, 8468 (1994)
- [66] S.-T. Lou, Z.-Q. Ouyang, Y. Zhang, X.-J. Li, J. Hu, M.-Q. Li, F.-J. Yang, *J. Vac. Sci. Technol. B Microelectron. Nanometer Struct. Process Meas. Phenom.* 18, 2573 (2000)
- [67] P.S. Epstein, M.S. Plesset, *J. Chem. Phys.* 18, 1505 (1950)
- [68] X.H. Zhang, N. Maeda, J. Hu, *J. Chem. Phys. Chem. B* 112, 13671 (2008)
- [69] R.P. Berkelaar, H.J.W. Zandvliet, D. Lohse, *Langmuir* 29, 11337 (2013)
- [70] S. Wang, L. Zhou, X. Wang, C. Wang, Y. Dong, Y. Zhang, Y. Gao, L. Zhang, J. Hu, *Langmuir* 35, 2498 (2019)
- [71] X.H. Zhang, N. Maeda, V.S.J. Craig, *Langmuir* 22, 5025 (2006)
- [72] V. Belova, M. Krasowska, D. Wang, J. Ralston, D.G. Shchukin, H. Mohwald, *Chem. Sci.* 4, 248 (2013)

## 6. Discussion of other scientific achievements

### 6.1 Description of research not contributing directly to the Habilitation thesis

#### 6.1.1 Research conducted prior to completing my doctoral studies

**D1. P. E. Theodorakis**, A. Avgeropoulos, J. J. Freire, M. Kosmas, C. Vlahos, “Effects of the chain architecture on the miscibility of symmetric linear/linear and star/star polymer blends”, *Macromolecules* 39, 4235 (2006)

**D2. P. E. Theodorakis**, A. Avgeropoulos, J. J. Freire, M. Kosmas, C. Vlahos, “Effective interaction parameter of linear/star polymer blends and comparison with that of linear/linear and star/star blends” *Journal of Chemical Physics* 126, 174904 (2007)

**D3. P. E. Theodorakis**, A. Avgeropoulos, J. J. Freire, M. Kosmas, C. Vlahos, “Monte Carlo simulation of star/linear and star/star blends with chemically identical monomers”, *Journal of Physics: Condensed Matter* 19, 466111 (2007)

**D4. S. Rangou, P. E. Theodorakis**, L. N. Gergidis, A. Avgeropoulos, P. Efthymiopoulos, D. Smyrniotis, M. Kosmas, C. Vlahos, “Synthesis, molecular characterization and theoretical study of first generation dendritic homopolymers of Butadiene and Isoprene with different microstructures”, *Polymer* 48, 652 (2007)

**D5. M. I. Papafaklis, C. V. Bourantas, P. E. Theodorakis**, C. S. Katsouras, D. I. Fotiadis, L. K. Michalis, “Coronary dilatation ten weeks after paclitaxel eluting stent implantation. No role of shear stress in lumen enlargement”, *Heart and Vessels* 22, 268 (2007)

**D6. M. I. Papafalis, C. V. Bourantas, P. E. Theodorakis**, C. S. Katsouras, D. I. Fotiadis, L. K. Michalis, “Association of endothelial shear stress with plaque thickness in a real three-dimensional left main coronary artery”, *International Journal of Cardiology* 115, 276 (2007)

#### Brief summary of publications D1–D6:

Articles D1–D3 are directly related to my doctoral thesis, while articles D4–D6 are associated with additional research tasks carried out during the studies. D1–D3 deal with the study of polymer blends with chains of variable architecture *via* Monte Carlo simulations based on the Bond Fluctuation Model. These studies involved two polymer architectures, namely the linear and the star architecture. Two distinct cases have been considered: i) polymer blends with monomers of the same chemical type [D3] and ii) polymer blends with monomers of different chemical types [D1–D2]. In both cases, we aimed at identifying the role of polymer-chain architecture on the miscibility of the blends. In case i), we have investigated the effect of the chain size and the architectural asymmetry on the miscibility of the blends. We have found that the increase of the volume fraction of star chains in star/linear blends increases the miscibility in the blends. On the contrary, an increase in the functionality of the star polymers decreases the miscibility in linear/star and star/star blends. An increase of the molecular weight (chain length) of linear chains leads to the decrease of the miscibility in linear/star blends. These findings have been compared with experimental and theoretical findings. In case ii) of polymer blends with linear and star chains with chemically distinct monomers, the aforementioned effects are opposite. In particular, linear/star blends are more miscible than the respective linear/linear blends, in agreement with experimental and theoretical results. Moreover, linear/star blends are less miscible than star/star blends, which verifies theoretical findings. Our results for both the blends with chains of the same and the blends with chemically different monomers indicate the way that the miscibility changes in those blends by using chains of linear or star architecture, which has important implications for the chemical industry. Owing to the scientific interest in various polymer architectures, we have also investigated the properties of dendrimer polymers in solutions, work that has taken place in collaboration with experiment and theory [D4]. Results on the experimentally synthesised dendrimer molecules and the theoretical results have been compared with our Monte Carlo simulations of the Bond Fluctuation Model and an off-lattice Monte Carlo method carried out by other colleagues in the same project. Our simulations have been able to characterise the structural properties of these macromolecules, whence the empty space in the interior of the dendritic macromolecule and the maximum size of guest molecules has been shown to be a non-monotonic function of the dendritic functionality.

Moreover, the increase of the branch length has been found to decrease this ability. These results have important consequences for drug delivery applications, where the dendrimers play the role of the carrier.

In another area of research, we have investigated the endothelial shear stress with plaque thickness in a real three-dimensional (3D) left main coronary artery, where computational methods were used to obtain the shear stress [D5, D6]. The real three-dimensional reconstruction of the left main coronary artery, left bifurcation, left anterior descending coronary artery and left circumflex coronary artery was reconstructed using biplane angiography and intravascular ultrasound imaging. The plaque thickness was calculated and by using computational fluid dynamics in the three-dimensional luminal model, the endothelial shear stress was computed. The main conclusion of the study [D5] has been that shear stress and plaque thickness were inversely related. Also, the 3D modelling of the arteries has enabled the study of the relationship of hemodynamic parameters with the plaque thickness in the critical coronary regions. This method has since then been applied on data obtained from various patients under different treatments. Another conclusion in a subsequent study [D6] has been that the neointimal thickness has been found as well to be inversely related to the shear stress without significant association of the tissue regression depth with the shear stress.

## 6.1.2 Research conducted after obtaining my PhD in Materials Science and Engineering

### 6.1.2.1 Research in computational medicine

**A1.** M. I. Papafaklis, C. V. Bourantas, **P. E. Theodorakis**, C. S. Katsouras, D. I. Fotiadis, L. K. Michalis, “Relationship of shear stress with in stent restenosis: bare metal stenting and the effect of brachytherapy”, *International Journal of Cardiology* 134, 25 (2009)

**A2.** M. I. Papafaklis, C. V. Bourantas, **P. E. Theodorakis**, C. S. Katsouras, K. K. Naka, D. I. Fotiadis, L. K. Michalis, “The effect of shear stress on neointimal response following sirolimus and paclitaxel-eluting stent implantations compared to bare metal stents in humans”, *Journal of American College of Cardiology: Cardiovascular Interventions* 3, 1181 (2010)

A1 and A2 are subsequent case studies as in D5 and D6.

### 6.1.2.2 Research in polymer physics

**B1.** **P. E. Theodorakis**, W. Paul, K. Binder, “Microphase separation in bottle-brush polymers under poor solvent conditions”, *EPL* 88, 63002 (2009)

**B2.** **P. E. Theodorakis**, W. Paul, K. Binder, “Pearl-necklace structures of molecular brushes with rigid backbone under poor solvent conditions. A simulation study”, *Journal of Chemical Physics* 133, 104901 (2010)

**B3.** **P. E. Theodorakis**, H.-P. Hsu, W. Paul, K. Binder, “Computer simulations of bottle-brush polymers with flexible backbones: Good solvent versus theta solvent conditions”, *Journal of Chemical Physics* 136, 164903 (2011)

**B4.** **P. E. Theodorakis**, N. G. Fytas, “Molecular Dynamics simulations of bottle-brush polymers with a flexible backbone under theta and good solvent conditions”, *American Journal of Condensed Matter Physics* 2, 101 (2012)

**B5.** N. G. Fytas, **P. E. Theodorakis**, “Molecular dynamics simulations of single-component bottle-brush polymers with a flexible backbone under poor solvent conditions”, *Journal of Physics: Condensed Matter* 25, 285105 (2013)

**B6.** **P. E. Theodorakis**, W. Paul, K. Binder, “Interplay between chain collapse and microphase separation in bottlebrush polymers with two types of side chains”, *Macromolecules* 46, 5137 (2010)

**B7.** **P. E. Theodorakis**, W. Paul, K. Binder, “Analysis of the cluster formation in two-component cylindrical bottle-brush polymers under poor solvent conditions. A simulation study”, *European Physical Journal E* 34, 52 (2011)

**B8.** I. Erukhimovich, **P. E. Theodorakis**, W. Paul, K. Binder, “Mesophase formation in two-component cylindrical bottle-brush polymers”, *Journal of Chemical Physics* 134, 054906 (2011)

- B9.** N. G. Fytas, **P. E. Theodorakis**, “Phase behavior of two-component bottle-brush polymers with flexible backbones under poor solvent conditions”, *Materials Research Express* 1, 015301 (2014)
- B10.** H. Maleki, **P. E. Theodorakis**, “Structure of bottle-brush brushes under good solvent conditions: A molecular dynamics study”, *Journal of Physics: Condensed Matter* 23, 505104 (2011)
- B11.** A. Chremos, **P. E. Theodorakis**, “Morphologies of bottle-brush block-copolymers”, *ACS Macro Letters* 3, 1096 (2014)
- B12.** A. Chremos, **P. E. Theodorakis**, “Impact of intrinsic backbone chain stiffness on the morphologies of bottle-brush diblock copolymers”, *Polymer* 97, 191 (2016)
- B13.** **P. E. Theodorakis**, N. G. Fytas, “Microphase separation in multiblock copolymers under poor solvent conditions”, *Soft Matter* 7, 1038 (2011)
- B14.** **P. E. Theodorakis**, N. G. Fytas, “Phase behavior of linear symmetric multiblock copolymers”, *EPL* 93, 43001 (2011)
- B15.** N. G. Fytas, **P. E. Theodorakis**, “Analysis of the static properties of cluster formations in symmetric linear multiblock copolymers”, *Journal of Physics: Condensed Matter* 23, 235106 (2011)
- B16.** **P. E. Theodorakis**, N. G. Fytas, “A Study of the static properties of symmetric linear multiblock copolymers under poor solvent conditions”, *Journal of Chemical Physics* 136, 094902 (2012)
- B17.** N. G. Fytas, **P. E. Theodorakis**, “Wang-Landau study of a square-well polymer chain”, *American Journal of Condensed Matter Physics* 3, 137 (2013)

#### Brief summary of publications B1–B17:

Following my doctoral studies, where Monte Carlo methods were used to study polymeric systems, I then continued working on polymer systems with off-lattice models by using molecular dynamics simulation based on coarse-grained models. Together with my collaborators, we have mainly dealt with three different systems: i) bottle-brush homo/copolymers under different solution conditions, ii) bottle-brush copolymer melts and iii) multiblock copolymers in solutions.

i) *Bottle-brush polymers in solutions:* We have used molecular dynamics simulations of a coarse-grained model to study the structure of bottle-brush homopolymers with rigid backbones [B1]. We have constructed the phase diagram of the different possible structures for these macromolecules based on structural parameters, such as the grafting density, the chain length, and the solvent quality (from poor to good solvent conditions). Our results have confirmed previous theoretical predictions (Sheiko et al. EPJE 13 (2004) 125) and have characterised the different structures in terms of various correlation lengths. In particular, the pearl-necklace structure at intermediate grafting densities has been characterised as well as the transitions between the possible different structures [B1]. The pearl-necklace structure of the brushes with rigid backbones under poor solvent conditions has been further analysed by studying the transition from the pearl-necklace structure to the axially uniform bottle-brush structure at high grafting density [B2]. These studies have been extended for bottle-brush polymers with flexible backbones under good and theta solvent conditions by using molecular dynamics and Monte Carlo simulation [B3]. The obtained results have indicated that chains are significantly stretched due to the tethering of the grafted chains with a weak dependence on the solvent quality. We have further characterised the structures by obtaining the effective persistence lengths, which has shown that different measures of the persistence length only agree in the case of Gaussian chains, otherwise mutually non-consistent results are obtained that depend both on the length of the backbone and the solvent quality. This has an important effect for a number of different systems, where the persistence length of a molecule needs to be considered [B3]. A more detailed study of the structural properties of bottle-brush polymers under theta, good, and poor solvent conditions has been conducted providing information on the persistence length of the brush backbone, and parameters that characterise the overall shape of the brushes (*e.g.* asphericity, acylindricity, *etc.*) [B4,B5].

Further studies in this area have also included the case of bottle-brush copolymers with rigid backbones, where grafted chains with different chemical types of chains alternate along the backbone [B6]. By varying the solvent quality and the grafting density, we have investigated the crossover from pearl-necklace structures at intermediate grafting densities to dense cylinders. We have also characterised the structure of these brushes for small grafting density identifying structures such as ‘dumbbells’ and short-range ‘Janus dumbbell’ configurations at larger grafting density. It has been found that all phase transitions occur gradually, due to the one-dimensional character of bottle-brush polymers with rigid backbones in comparison with sharp phase transitions that occur in the case of bulk polymer mixtures or block copolymer melts [B6]. Furthermore, we have characterised the shape of the pearl-necklace structures in the case of bottle-brush copolymers with rigid backbones and compared these results with the case of single-component bottle-brush polymers [B7]. In general, the possible types of ordering in the case of bottle-brush copolymers with rigid backbones are reminiscent of the ordering of block copolymers in cylindrical confinement [B8]. Hence, the simulations could be compared with a generalised Leibler’s theory of microphase separation in block copolymer melts, which provides a description at the weak segregation limit. The comparison between simulation and theory was carried out on the basis of suitable correlation functions, which were able to identify the conditions when Janus-cylinder-type ordering and when microphase separation in the direction along the rigid backbone of the bottle-brush polymers occurred. This study has provided evidence for a short-range order due to a tendency of microphase separation in the axial direction, with a wavelength proportional to the radius of gyration of the side chains. Most importantly, this length scale is independent of the temperature and the grafting density for a wide range of parameters considered in the study [B8]. Bottle-brush symmetric copolymers with two types of side chains with flexible backbones have been also considered in our studies [B9]. It has been found that the Janus and pearl-necklace structures described in the previous studies are fully attributed to the rigidity of the backbone of the brushes under poor solvent conditions and concluded that such structures are unlikely in bottle-brushes with fully flexible backbones. We have further determined the phase diagram of structures for bottle-brush copolymers with flexible backbones and enabled their comparison with the rigid backbone cases [B9]. Our work on bottle-brush polymers in solution conditions has been concluded by studying a more complex architecture of bottle-brush polymers, namely bottle-brush brush homopolymers with rigid backbones, where the side chains exhibit the bottle-brush architecture [B10]. By carrying out a parametric study, the structural properties of these complex macromolecules have been characterised and it has been found that pearl-necklace structures are not possible as in the case of bottle-brush homopolymers because the brush-like structure of the side chains stretches the chains in the radial direction from the backbone [B10].

ii) *Bottle-brush copolymer melts*: These systems can form periodic morphologies, which are relevant in diverse and expanding range of practical applications, such as drug delivery, microelectronics, and other advanced materials [B11]. By using extensive molecular dynamics simulations, we have obtained the morphology diagrams of bottle-brush copolymers (symmetric in composition) [B11]. We have found that molecular asymmetry (asymmetry of side chain lengths) can lead to the formation of cylindrical domains, which deviates significantly from what is expected for linear block copolymers. Moreover, bottle-brush copolymers have demonstrated faster self-assembly and enabled asymmetric domain spacings in the case of lamellar structures in comparison with the respective linear copolymer chains. In this respect, our study has provided detailed morphology maps for these systems, in this way guiding the design of experimentally achievable structures for nanoporous and photonic materials based on the self-assembly of bottle-brush block copolymers [B11]. In a follow-up study [B12], we have demonstrated that the hexagonal cylindrical morphology is accessible to the systems when the backbone of the bottle-brush molecules is flexible. When the intrinsic backbone stiffness of the bottle-brush copolymer chains increases beyond a threshold that depends on the particular choice of parameters for the brush molecules, an order–order transition from hexagonally packed cylinders to lamellar morphologies with asymmetric domain spacings would take place. This is particularly important for nanopatterning and semiconductor applications [B12].

iii) *Multiblock copolymers in solution conditions*: We have studied linear multiblock copolymer chains in dilute solution conditions by using molecular dynamics simulations of a coarse-grained model on a path to understand more complicated processes, which could potentially involve biological processes, such as protein folding. In this case, the architecture of the chain was linear, but the chain consisted of two different types of chemical units that alternated periodically along the chain. The volume fraction of the two types of beads of the chain was the same. We have identified the possible structures of these molecules, namely, coil structures at higher temperatures, and characterised the formation of different clusters as the temperature decreases emulating poor solvent conditions, which results in the microphase separation between unlike beads [B13]. A detailed phase diagram has been obtained that includes the different scenarios (structure map) as a function of temperature, and the number and the length of the copolymer blocks [B14]. In summary, three different cases were observed: a) the full microphase separation between the blocks of different type b) the full microphase separation with a certain probability, and c) cases where the full microphase separation cannot take place [B14]. A detailed analysis of the structure of the microphase separated clusters, which includes their dimensions and shape, as well as properties of the individual blocks has been provided for different solvent conditions [B15, B16].

### 6.1.2.3 Research in soft matter systems with colloids

**C1. P. E. Theodorakis**, C. Dellago, G. Kahl, “A coarse-grained model for DNA-functionalized spherical colloids, revisited: Effective pair potential from parallel replica simulations”, *Journal of Chemical Physics* 138, 025101 (2013)

**C2. P. E. Theodorakis**, N. G. Fytas, G. Kahl, C. Dellago, “Self-assembly of DNA-functionalized colloids”, *Condensed Matter Physics* 18, 22801 (2015)

**C3. P. Yatsyshin**, N. G. Fytas, **P. E. Theodorakis**, “Mixing–demixing transition in polymer-grafted spherical nanoparticles”, *Soft Matter* 16, 703 (2020)

#### Brief summary of publications C1–C3:

Here, the focus has been on the self-assembly of systems of colloids with tethered chains, which were either DNA or polymer chains. These systems enable property profiles and morphologies that are not possible to obtain by using only colloids and polymers or colloids and DNA chains. This work has implications for multiple technological areas in materials science, medicine and beyond. In the context of DNA-coated colloids, we have reviewed this area and revisited a proposed coarse-grained model for these molecular complexes and characterised in detail the transition from bonded to unbonded configurations by using an in-house parallel Monte Carlo off-lattice algorithm. This transition was found to take place at much lower temperatures than it was initially believed [C1,C2]. We also found that an increasing colloid size hinders the hybridisation of the DNA strands, in agreement with experimental findings [C1]. The phase behaviour of polymer-coated colloids was studied by extensive molecular dynamics simulation of a coarse-grained model [C3]. In this case, we have considered the most symmetric case of polymer-coated colloid melts in order to isolate the most crucial elements that determine the mixing-demixing transition in these systems. This study has identified two key features of these systems: a) the increase of the colloid size hinders the demixing of the system, and b) for intermediate colloid sizes, the increase of the grafting density can initially favour demixing, but further increase makes demixing more difficult. This is due to the increase of an effective core that forms as the grafting density of the tethered chains around the colloids increases [C3]. These key features are important for materials design in systems of polymer-grafted nanoparticles.

### 6.1.2.4 Research in spin systems

**E1. N. G. Fytas**, **P. E. Theodorakis**, “Universality in disordered systems: The case of the  $d=3$  random bond Ising model”, *Physical Review E* 82, 062101 (2010)

**E2. P. E. Theodorakis**, N. G. Fytas, “Wang-Landau study of the 3D Ising model with bond disorder”, *European Physical Journal B* 81, 245 (2011)

- E3.** N. G. Fytas, **P. E. Theodorakis**, “Universality aspects of the 2d random-bond Ising and 3d Blume-Capel models”, *European Physical Journal B* 86, 30 (2013)
- E4.** **P. E. Theodorakis**, N. G. Fytas, “Monte Carlo study of the triangular Blume-Capel model under bond randomness”, *Physical Review E* 86, 011140 (2012)
- E5.** N. G. Fytas, J. Zierenberg, **P. E. Theodorakis**, M. Weigel, W. Janke, A. Malakis, “Universality from disorder in the random-bond Blume–Capel model”, *Physical Review E* 97, 040102(R) (2018)
- E6.** N.G. Fytas, A. Mainou, **P. E. Theodorakis**, A. Malakis, “Monte Carlo study of the interfacial adsorption of the Blume–Capel model”, *Physical Review E* 99, 012111 (2019)
- E7.** E. Vatanserver, Z. D. Vatansever, P. E. Theodorakis, N. G. Fytas, “Ising universality in the two-dimensional Blume-Capel model with quenched random crystal field”, *Physical Review E* 102, 062138 (2020)
- E8.** N. G. Fytas, **P. E. Theodorakis**, I. Georgiou, “Universality aspects of the trimodal random-field Ising model” *European Physical Journal B* 85, 349 (2012)
- E9.** **P. E. Theodorakis**, N. G. Fytas, “Specific heat exponent of random-field Ising magnets”, *American Journal of Condensed Matter Physics* 3, 9 (2013)
- E10.** **P. E. Theodorakis**, I. Georgiou, N. G. Fytas, “Fluctuations and criticality in the random-field Ising model”, *Physical Review E* 87, 032119 (2013)
- E11.** N. G. Fytas, **P. E. Theodorakis**, I. Georgiou, I. Lelidis, “Critical aspects of the random-field Ising model”, *European Physical Journal B* 86, 268 (2013)
- E12.** **P. E. Theodorakis**, N. G. Fytas, “Random-field Ising model: insight from zero-temperature simulations”, *Condensed Matter Physics*, 17, 43003 (2014)
- E13.** N. G. Fytas, **P. E. Theodorakis**, A. K. Hartmann, “Revisiting the scaling of the specific heat of the d=3 random-field Ising model”, *European Physical Journal B* 89, 200 (2016)
- E14.** N. G. Fytas, **P. E. Theodorakis**, “Universality in four-dimensional random-field magnets”, *European Physical Journal B* 88, 205 (2015)
- E15.** N. G. Fytas, **P. E. Theodorakis**, A. Malakis, “Interfacial adsorption in 2D pure and random-bond Potts models”, *Physical Review E* 95, 032126 (2017)

Brief summary of publications E1–E15:

The research on spin models with disorder included: i) the random-bond Ising model, ii) the Blume-Capel model, iii) the random-field Ising model and iv) the random-bond Potts model. The main aim has been to characterise the universality class of these models and probe the critical behaviour of magnets that the models represent (in terms of critical exponents and universal ratios).

i) *Random-bond Ising model:* In the case of the three-dimensional (**3D**) random-bond Ising model, results based on extensive standard and Wang-Landau Monte Carlo simulations and finite-size scaling techniques have indicated that the universality of this system is the same as in the case of the site- and the bond-diluted models, which is clearly distinct from that of the pure Ising model [E1,E2]. The above three models provide a complete set of universality in disordered systems [E1,E2]. The Wang-Landau studies were then expanded in the cases of the two-dimensional (2D) random-bond Ising model and the 3D Blume–Capel model at zero crystal-field coupling [E3]. This study has verified the theoretically predicted strong universality hypothesis for the 2D random-bond Ising model, while for the 3D Blume–Capel model, the universality class of the 3D Ising has been verified for the second-order regime [E3].

ii) *Blume–Capel model:* The investigations of the 2D triangular Blume–Capel model under bond randomness in its first- and second-order phase-transition regimes and finite-size scaling analysis have been conducted [E4]. Regarding the second-order regime, the second-order phase transition has been found to emerge from the second-order regime of the pure model under randomness, what is compatible with the universality class of the 2D random Ising model, reinforcing the scenario of strong universality in the 2D Ising model with quenched disorder. The same is true when the second-

order transition emerges from the first-order regime of the pure model. These results are in agreement with renormalisation-group calculations [E4]. The effects of quenched disorder in the exchange couplings of the Blume–Capel model on the square lattice have been studied by Monte Carlo simulation and finite-size scaling analysis. It has been concluded that the first-order transition softens to become continuous with a divergent correlation length [E5]. Further analysis has shown that this model belongs to the universality class of the Ising model with additional logarithmic corrections, which is also observed in the Ising model if coupled to weak disorder [E5]. These studies were extended to investigate the interfacial adsorption of the pure Blume-Capel model at the first- and second-order transition regimes and at the vicinity of the tricritical point, confirming predictions from analytic free-energy scaling arguments [E6]. The study also considered the interfacial adsorption under quenched bond randomness at the originally first-order transition regime and relevant self-averaging properties of the system. The results have indicated that transient effects were present, supporting the scenario of a non-divergent scaling as in the case of the original second-order transition regime of the pure model [E6]. Recently, a parallel version of the Wang-Landau algorithm was implemented to investigate the effect of quenched disorder in the crystal-field coupling of the Blume-Capel model on a square lattice [E7]. In the regime that the pure model undergoes a continuous transition, finite-size scaling analysis provided evidence in favour of the strong universality hypothesis with the presence of additional logarithmic corrections in the scaling of the specific heat. In the regime where the pure model undergoes a first-order phase transition, it has qualitatively been shown that there is a smoothing of the transition to second-order with the presence of strong scaling corrections [E7].

iii) *Random-field Ising model*: The investigations of the critical properties of the 3D trimodal random-field Ising model with an equal weight trimodal distribution at zero temperature were conducted by using graph-theoretical algorithm (Push-Relabel algorithm) [E8]. This algorithm enabled us to study system sizes up to  $N=128^3$  ( $N$  is the total number of spins). Based on the sample-to-sample fluctuations of the order parameter and finite-size scaling methods the critical parameters have been calculated, namely the critical disorder strength and the critical exponent of the correlation length and the order parameter, which placed this model in the same universality class with the corresponding Gaussian random-field Ising model [E8]. For the latter system, the specific heat exponent has been determined, in agreement with experimental measurements on random-field and diluted antiferromagnetic systems and previous simulations [E9]. The push-relabel algorithm has been used to study the fluctuations and criticality of the 3D random-field model with a Gaussian distribution at zero temperature for lattice size  $L \leq 156$  [E10–E12]. Using a novel method for the sample-to-sample fluctuations, the fourth-order Binder cumulant, and finite-size scaling analysis, the critical disorder strength,  $h_c$ , and the critical exponent  $\nu$  were estimated. The obtained results have suggested limiting bounds for the critical exponent,  $\alpha$ , and the violation of the hyperscaling exponent,  $\theta$ . Based on a data collapse analysis of the order parameters and the disconnected susceptibility, we have found accurate estimates for the  $\beta/\nu$  and the  $\bar{\gamma}/\nu$  critical exponent ratios [E10–E12]. The scaling behaviour of the specific heat of the 3D random-field Ising model with a Gaussian distribution of the disorder, which has been a highly controversial issue, was investigated for large systems, namely  $N=268^3$  spins [E13]. The specific heat-like quantity was defined by differentiating the bond energy with respect to the field,  $h$ , which is found to converge to a constant at the thermodynamic limit. As a by-product of the study, more accurate values for the critical field  $h_c=2.279(7)$  and the critical exponent of the correlation exponent  $\nu=1.37(1)$  have been obtained, which are the most accurate estimates in the literature and are in agreement with most of other results [E13]. Finally, by using zero-temperature numerical simulations, the 4D random-field Ising model has been studied by considering two distributions, namely the Gaussian and the equal-weight trimodal random-field Ising model [E14]. By using large ensembles of disorder realisations for both models for a broad range of random-field values and system sizes, the analysis based on sample-to-sample fluctuations and finite-size scaling has provided accurate estimates for the critical field,  $h_c$ , and the critical exponent,  $\nu$ , of the correlation length. The main conclusion has been that both models in four dimensions belong to the same universality class [E14].

iv) *Random-bond Potts model*: Monte Carlo simulations were used to analyse the finite-size scaling behaviour of the interfacial adsorption of the 2D square-lattice  $q$ -states Potts model, where the pure and random-bond versions of the

Potts model for  $q=3, 4, 5, 8,$  and  $10$  were considered [E15]. In this way, it was possible to investigate the properties of the originally continuous, weak, and strong first-order phase transitions. While the results for the pure model have reproduced the early scaling predictions of the interfacial adsorption for both the first and the second-order phase transitions, in the random-bond case, the interfacial adsorption at the (disordered induced) continuous transition was considered by using scaling arguments and estimating self-averaging properties of the interfacial adsorption based on the infinite limit-size extrapolation of properly defined signal-to-noise ratios, which has shown that self-averaging is restored at the thermodynamic limit [E15]. For the pure and the random models, the isotropic finite-size scaling description for the interfacial adsorption of the continuous phase transition has been verified. For the pure  $q>4$  systems that undergo a first-order transition, we have probed the linear divergence of the interfacial adsorption [E15].

### 6.1.2.5 Research in biological physics

**G1.** A. B. Poma, M. Cieplak, **P. E. Theodorakis**, “Combining the MARTINI and structure-based coarse-grained approaches for the molecular dynamics studies of conformational transitions in proteins”, *Journal of Chemical Theory and Computation* 13, 1366 (2017)

**G2.** A. B. Poma, M. S. Li, **P. E. Theodorakis**, “Generalization of the elastic network model for the study of large conformational changes in biomolecules”, *Physical Chemistry Chemical Physics* 20, 17020 (2018)

**G3.** A.B. Poma, H. A. Vargas-Guzman, M. S. Li, **P. E. Theodorakis**, “Mechanical and thermodynamic properties of  $A\beta_{42}$ ,  $A\beta_{40}$  and  $\alpha$ -synuclein fibrils: A coarse-grained method to complement experimental studies”, *Beilstein Journal of Nanotechnology* 10, 500 (2019)

**G4.** S. Boopathi, D. Q. H. Pham, W. Gonzalez, **P. E. Theodorakis**, M. S. Li, “Zinc binding promotes greater hydrophobicity in Alzheimer’s  $A\beta_{42}$  peptide than copper binding: Molecular dynamics and solvation thermodynamics studies”, *Proteins: Structure, Function, Bioinformatics* 88, 1285 (2020)

**G5.** **P. E. Theodorakis**, E. A. Müller, R. V. Craster, O. K. Matar, “Physical insights into the blood–brain barrier translocation mechanisms”, *Physical Biology* 14, 041001 (2017)

**G6.** N. Q. Thai, **P. E. Theodorakis**, M. S. Li, “Fast estimation of the blood–brain barrier permeability by pulling a ligand through a lipid membrane”, *Journal of Chemical Information and Modeling* 60, 3057 (2020)

#### Brief summary of publications G1–G6:

Research in the area of biophysics includes two newly developed coarse-grained models for proteins [G1, G2], the study of protein fibrils, which are relevant for Alzheimer’s and Parkinson’s diseases [G3, G4], a review article on the blood–brain barrier physical translocation mechanisms [G5] and a method for estimating its permeability [G6].

We have developed the GoMARTINI model, which enables one of the most popular state-of-the-art coarse-grained force-fields (*i.e.* MARTINI [Monticelli *et al.* *J. Chem. Theory Comput.* 4, 819 (2008)]) to be successfully used for studying proteins undergoing large conformation changes (*e.g.* protein folding/unfolding) [G1]. The use of the elastic network was hindering the study of such phenomena with the MARTINI force-field. In the new model, we have substituted the elastic network with  $G\bar{o}$ -type model-approaches for the contacts between amino acids, which are based on the contact map of the native state of the protein [Sułkowska and Cieplak, *Biophys. J.* 95, 3174 (2008)]. To this end, our approach was able to offer better results for a number of structural measures for all investigated proteins [G1]. Then, the idea of enabling a standard elastic network model to be used for studying large configurational changes in proteins has emerged [G2]. In practice, we have extended the capabilities of the elastic network model by substituting the harmonic potentials for far contacts with *Lennard-Jones* potentials based on  $G\bar{o}$ -type contact maps of the native state. The results have been in agreement with the original elastic network model, while demonstrating the advantage of the new model in simulating large conformational changes, such as protein stretching and folding [G2]. This simple and efficient model is suitable for investigating many phenomena for proteins, which involve structural changes. Based on previous experience with coarse-grained models for polymers, we have used a  $G\bar{o}$ -type model to investigate a number

of biopolymers such as fibrils relevant for neurodegenerative diseases (*e.g.* Alzheimer's disease, *etc.*) with molecular dynamics simulation [G3]. These systems were  $\beta$ -amyloids ( $A\beta_{40}$ ,  $A\beta_{42}$ ) and  $\alpha$ -synuclein fibrils. The aim was to characterise the mechanical and thermodynamic properties of these fibrils. The model was able to provide estimates for elastic constants characterising the mechanical properties of these systems, allowing to identify a link between mechanical stability and aggregation tendency of these self-assembling proteins. The results have indicated that  $\alpha$ -synuclein fibrils are thermally less stable than  $\beta$ -amyloid fibrils [G3]. Further study on  $\beta$ -amyloid considered the effect of zinc and copper ions on the protein's properties and its ramification for aggregation [G4]. Finally, the [G5] review paper discussed the physical translocation mechanisms of the blood–brain barrier (BBB) which is a crucial topic in the context of neurodegenerative diseases. To this end, a fast and reliable method to estimate the permeability of the BBB by pulling ligands through a membrane has been proposed in [G6].

### 6.1.3 Other publications

- O1.** B. Liu, S. W. Wang, L. Chai, G. El Achkar, A. Chen, **P. E. Theodorakis**, “Experimental investigation of nanoparticles distribution mechanisms and deposition patterns during nanofluid droplet evaporation”, *European Physical Journal – Applied Physics* 92, 11101 (2020)
- O2.** H.-P. Hsu, W. Paul, **P. E. Theodorakis**, K. Binder, “Phase transitions and relaxation processes in macromolecular systems”, ed. G. Münster, D. Wolf, K. Kremer, *NIC Jülich, IAS Series* 3, 263–270 (2010)
- O3.** **P. E. Theodorakis**, W. Paul, K. Binder, “Diagram of states of bottlebrush polymers under poor solvent conditions”, *ACS POLY* 51, 452 (2010)
- O4.** M. Papafaklis, C. Bourantas, **P. Theodorakis**, C. Katsouras, D. Fotiadis, L. Michalis, “Association of endothelial shear stress with the type of atherosclerotic lesions in angiographically normal coronary arteries”, *Atherosclerosis* 7 (Supplements), 265 (2006)
- O5.** M. I. Papafaklis, C. V. Bourantas, **P. E. Theodorakis**, C. S. Katsouras, D. I. Fotiadis, L. K. Michalis, “Shear stress and prediction of neointima distribution: Sirolimus-eluting stents versus bare metal stents”, *American Journal of Cardiology* 98, 174M–175M (2006)

### 6.2 Oral presentations

#### Seminars:

- I1.** “*On the mechanisms of superspreading*”, Institute of Physics – Polish Academy of Sciences, **Warsaw** (13 Oct 2020)
- I2.** “*Molecular dynamics simulations of fluid flows on solid substrates*”, University of Ioannina, **Ioannina** (19 Feb 2020)
- I3.** “*Formation, dissolution and properties of surface nanobubbles: Insight from molecular dynamics simulation*”, IUTAM Symposium 2019: Computational modelling of instabilities and turbulence in separated tow-phase flows, **Dublin** (10 – 12 June 2019)
- I4.** “*Introduction to Molecular Dynamics simulation and examples*”, Tianjin University of Commerce, **Tianjin** (13 Mar 2019)
- I5.** “*Steering fluid motion with Gradient Substrates*”, Imperial College London, **London** (31 Jan 2019)
- I6.** “*Recognising the values and opportunities in Academia: A personal view*”, Imperial College London, **London** (31 Jan 2019)
- I7.** “*Steering fluid motion with gradient substrates*”, International symposium on data cooling and ThermaSMART annual workshop, **Tianjin** (3 – 5 Dec 2018)
- I8.** “*Molecular Dynamics simulation: Two applications of coarse-grained models for droplets on solid substrates*”, Tianjin University, **Tianjin** (23 Nov 2018)
- I9.** “*Stiffness-guided motion of a droplet on a solid substrate*”, National and Kapodistrian University of Athens, **Athens** (21 Mar 2018)

- I10.** “*Stiffness-guided motion of a droplet on a solid substrate*”, Institute of Physics – Polish Academy of Sciences, **Warsaw** (6 Mar 2018)
- I11.** “*Using the contact map in the MARTINI and Elastic Network models to study large conformation changes in proteins*”, CNRS Laboratory of Theoretical Biochemistry, **Paris** (9 Nov 2017)
- I12.** “*Combining the MARTINI and structure-based coarse-grained approaches for the molecular dynamics studies of conformational transitions in proteins*”, Skype seminar ICST **HCM City** (25 Nov 2016)
- I13.** “*Morphologies of Bottle-brush block copolymers*”, Coventry University, **Coventry** (9 Mar 2016)
- I14.** “*Self-assembly of DNA-coated colloids*”, Institute of Physics – Polish Academy of Sciences, **Warsaw** (18 Feb 2015)
- I15.** “*Design of novel functional materials with computer simulations*”, University College London, **London** (2 Dec 2014)
- I16.** “*Numerical studies and design of novel functional materials*”, Coventry University, **Coventry** (16 Sep 2014)
- I17.** “*How superspreading works? Understanding the mechanism with molecular dynamics simulations*”, Coventry University, **Coventry** (28 May 2014)
- I18.** “*Understanding the superspreading mechanism of surfactant-laden flows via a combined molecular and continuum approach*”, Coventry University, **Coventry** (10 Jul 2013)
- I19.** “*An overview of the properties of complex macromolecules: the case of bottle-brush and multi-block copolymers and the self-assembly of DNA-coated colloids*”, FU Berlin, **Berlin** (11 Apr 2012)
- I20.** “*DNA as a material: Recent advances by computer simulations*”, Adam Mickiewicz University of Poznań, **Poznań** (13 Oct 2011)
- I21.** “*Recent advances in soft matter: theory, simulations and applications*”, University of Ioannina, **Ioannina** (13 May 2011)
- I22.** “*Soft matter: from complex systems to coarse-grained models*”, Johannes Gutenberg-University, **Mainz** (3 May 2011)
- I23.** “*Microphase separation in multiblock copolymers under poor solvent conditions*”, Technical University of Vienna, **Vienna** (15 Dec 2010)
- I24.** “*Mesophase formation in two-component cylindrical bottle-brush polymers under poor solvent conditions*”, National Technical University of Athens, **Athens** (13 Sep 2010)
- I25.** “*Molecular dynamics simulations of bottlebrush polymers under poor solvent conditions*”, ETH Zürich, **Lugano** (8 Jul 2010)
- I26.** “*Molecular dynamics simulations of bottlebrush polymers under poor solvent conditions*”, University of Vienna, **Vienna** (23 Jun 2010)
- I27.** “*Bottlebrush polymers under poor solvent conditions*”, Massachusetts Institute of Technology, **Boston** (22 Apr 2010)
- I28.** “*Interplay between chain collapse and microphase separation in bottlebrush polymers under poor solvent conditions*”, University of Ioannina, **Ioannina** (10 Mar 2010)
- I29.** “*Microphase separation of bottle-brush polymers under poor solvent conditions*”, Johannes Gutenberg-University, **Mainz** (22 Dec 2009)
- I30.** “*Microphase separation of bottle-brush polymers under poor solvent conditions*”, Martin-Luther University, **Halle** (15 Dec 2009)

#### **Workshops and school conferences:**

- W1.** “*Molecular dynamics simulation of fluid flows*”, one-day workshop at Dalian Maritime University, **Dalian** (16 July 2019)
- W2.** “*Molecular dynamics simulation of fluid flows*”, 4<sup>th</sup> workshop on advances in CFD, LB and MD modelling of capillary two-phase flows and experimental validation, **Rio de Janeiro** (16–19 May 2019)

- W3.** “*Stiffness-guided motion of a droplet on a solid substrate*”, 3<sup>rd</sup> workshop of Vietnamese students in Poland, **Warsaw** (6–7 Sep 2018)
- W4.** “*Team-working: Moving forward and Enjoying science together*”, NGSchool2017 10–17 September 2017, **Warsaw** (14 Sep 2017)
- W5.** “*Superspreading: insights from molecular-level simulations*”, Summer school, Centre for Doctoral Training on Fluid Dynamics across scales, 11–15 July 2016, **London** (13 Jul 2016)
- W6.** “*The superspreading mechanism unveiled via molecular dynamics simulations*”, Workshop entitled “Computer simulation of confined fluids”, The shard, **London** (8 Dec 2014)
- W7.** “*Multi-scale analysis of surfactant-assisted superspreading*”, OCCAM, University of Oxford, **Oxford** (22 Jul 2013)
- W8.** “*Self-assembling DNA-coated colloids. A simulation study*”, Workshop for Austrian SFB meeting, **Vienna** (28–29 Apr 2011)
- W9.** “*Mesophase formation in bottle-brush polymers under poor solvent conditions. A molecular dynamics study*”, Workshop for Austrian “Kickoff” ViCoM Meeting, **Burg Schlaining** (28–29 Oct 2010)
- W10.** “*Molecular dynamics simulations of bottlebrush polymers under poor solvent conditions*”, International workshop “Theory and Computer Simulation of Polymers: New Developments”, **Moscow** (31 May–6 Jun 2010)
- W11.** “*Polymer brushes under poor solvent conditions*”, Winter School Conference “Polymers under Constraints: Theory, Experiments, Simulations”, **Titisee** (31 Jan–5 Feb 2010)

#### **Conferences and meetings:**

- M1.** “*Stiffness-guided motion of a droplet on a solid substrate*”, APS Division of Fluid Dynamics 2019, **Seattle** (23–26 November 2019)
- M2.** “*Formation, dissolution and properties of surface nanobubbles*”, International Conference of Multiphase Flow 2019, **Rio de Janeiro** (19–24 May 2019)
- M3.** “*Superspreading: molecular dynamics simulations and experimental results*”, APS Division of Fluid Dynamics, **Boston** (22–24 Nov 2015)
- M4.** “*Superspreading: Mechanisms and molecular design*”, Mainz Materials Simulations Days, **Mainz** (10–12 Jun 2015)
- M5.** “*The superspreading mechanism unveiled via molecular dynamics simulations*”, APS Division of Fluid Dynamics, **San Francisco** (23–25 Nov 2014)
- M6.** “*Multi-scale approach to studying super-spreading: molecular dynamics and continuum level models*”, APS Division of Fluid Dynamics, **Pittsburgh** (24–26 Nov 2013)
- M7.** “*Engineering and control of surfactant-laden flows: experiments and MD simulations*”, APS Division of Fluid Dynamics, **Pittsburgh** (24–26 Nov 2013)
- M8.** “*A multi-scaling approach for the study of surfactant-laden flows*”, SoftComp Annual Meeting, **Rimini** (27–30 May 2013)
- M9.** “*Effect of the chain architecture in linear/linear and star/star symmetric binary polymer blends*”, XXII Panhellenic Congress of Solid-State Physics and Materials Science, **Patras** (24–27 Sep 2006)

#### **6.3 Principal investigator of research projects at IPPAS**

- P1.** Polonez-1 NCN (ID: 2015/19/P/ST3/03541): “Self-aggregation of protein complexes: virus capsids and amyloids”
- P2.** H2020-MSCA-RISE-2017 (ID: 778104): “Smart thermal management of high-power microprocessors using phase-change”
- P3.** Sonata-Bis-9 NCN (ID: 2019/34/E/ST3/00232): “Controlling Fluids with Surfactant: Multiscale exploration of topological changes”

**P4.** Opus-18 NCN (ID: 2019/35/B/ST3/03426): “Directing fluid motion with gradient substrates”

#### **6.4 Fellowships and awards**

**F1.** Granty na granty (2020)

**F2.** Marie Skłodowska-Curie Fellow (2016–2018)

**F3.** Premia na Horyzoncie (2018)

**F4.** Outstanding contribution in reviewing, Journal of Colloid & Interface Science, Elsevier (2016)

**F5.** Max Planck Fellow (2008–2010)

**F6.** 4 journal covers (Soft Matter, Langmuir, European Physical Journal E, Journal of Physics: Condensed Matter)

#### **6.5 Research visits (minimum 1 month)**

**V1.** Kyushu University (**Japan**, 11–12/2019)

**V2.** Kobe University (**Japan**, 10–11/2018)

**V3.** Massachusetts Institute of Technology (**USA**, 03–04/2010)

**V4.** Tianjin University of Commerce (**China**, 11–12/2018, 02–03/2019, 09–10/2019)

**V5.** Tianjin University (**China**, 11–12/2018, 02–03/2019, 09–10/2019)

**V6.** Dalian Maritime University (**China**, 06–07/2019)

**V7.** Federal University of Rio de Janeiro (**Brazil**, 05–06/2019)

#### **6.6 Visiting Researcher**

02/2017 – present: Centre for Fluid and Complex Systems, Department of Mathematics and Physics, Coventry University, **United Kingdom**

### ***7. Service to academic community***

#### **7.1 Reviewer activity**

- projects for: NSF (USA), NWO (Netherlands), EPSRC (UK)

- articles for research journals: Nano Letters, Macromolecules, ACS Macro Letters, Journal of Chemical Theory and Computation, Journal of Chemical Education, Soft Matter, AIP Advances, Journal of Physics: Condensed Matter, Physica Scripta, American Journal of Condensed Matter Physics, Journal of Physical Chemistry, Condensed Matter Physics, Journal of Physics D: Applied Physics, RCS Advances, Quantitative Finance, Journal of Colloid and Interface Science, Langmuir, Applied Surface Science, Journal of Chemical Physics, Journal of Physics A: Mathematical and Theoretical, PLoS ONE, Physical Chemistry Chemical Physics, Fluid Phase Equilibria, Journal of Molecular Liquids, Particulate Science and Technology, International Journal for Numerical Methods in Biomedical Engineering, Entropy, Acta Physica Polonica A, Applied Sciences, Computational Materials Science, Colloids and Surfaces A: Physicochemical and Engineering Aspects, International Journal of Heat and Mass Transfer, Cryogenics, Colloids and Interfaces, Powder Technology, Applied Thermal Engineering, Journal of Magnetism and Magnetic Materials, Materials, Fluids, Coatings, Scientific Reports, Crystals, Toxins, Mathematics, Physica A, Open Journal of Physical Chemistry, Case Studies in Thermal Engineering, International Journal of Molecular Sciences

- contributions for conferences: XII International Conference on Computational Heat, Mass, and Momentum Transfer 2019 (ICCHMT)

## 7.2 Memberships

- American Chemical Society (since 2013)
- American Physical Society (2019–2020)

## 7.3 Teaching activities

### 7.3.1 Teaching courses for PhD students at IPPAS and the Warsaw PhD School

- T1.** Learning Python: from beginner's to advanced level, (2021, Role: Course Leader, 22 hours)
- T2.** Learning Python: from beginner's to advanced level, (2020, Role: Course Leader, 19 hours)
- T3.** Theory of molecular-level simulations in materials science, fluid dynamics, and biology, (2019, Role: Course Leader, 24 hours)
- T4.** Computational Biophysics & Materials Science, (2019, Role: Course Leader, 12 hours)
- T5.** Computational Methods in Materials' Science and Biology, (2017, Role: Course Leader, 6 hours)
- T6.** Computational Methods in Materials' Science, (2017, Role: Course Leader, 24 hours)
- T7.** Statistical Thermodynamics in Soft Matter and Biological Physics, (2016, Role: Course Leader, 12 hours)

### 7.3.2 Mentorship of researchers and PhD students at IPPAS

- S1.** Mr Luís Henrique Carnevale da Cunha (PhD student, since 01/2021, supported by **P3** project)
- S2.** Mr Russell Kajouri (PhD student, since 11/2020, supported by **P4** project)
- S3.** Mr Soheil Arbabi (PhD student, since 10/2019, supported by IPPAS and **P3** project)
- S4.** Dr Adolfo Poma (Researcher, 11/2017–09/2018, supported by **P1** project)
- S5.** Ms Yuliia Varenky (Researcher, 12/2017–09/2018, supported by **P1** project)

## 7.4 Participation in Examining Committees

- X1.** Master's thesis of Mr Luís Henrique Carnevale da Cunha (State University of Rio de Janeiro, 15 Dec 2020)
- X2.** PhD thesis of Ms Kalliopi Miliou (University of Ioannina, 11 January 2021)

## 7.5 Activity as an editor

- Guest editor of special issue in *Materials*: "Modeling of structure formation in soft materials"
- Member of the editorial board of the American Journal of Condensed Matter Physics

## 7.6 Activities popularising science

Member of the DoScience team (since 2017)



.....  
(applicant's signature)